J. Nonlinear Sci. Vol. 10: pp. 291–331 (2000)
DOI: 10.1007/s003329910012

Journal of
Nonlinear
Science

Nonfocusing Instabilities in Coupled, Integrable Nonlinear Schrödinger pdes

M. G. Forest,[1,*] D. W. McLaughlin,[2,†] D. J. Muraki,[2,‡] and O. C. Wright[1,§]

[1] Department of Mathematics, The University of North Carolina at Chapel Hill, Chapel Hill, NC 27599-3250, USA

[2] Courant Institute of Mathematical Sciences, New York, NY 10012, USA

Received February 9, 1999; accepted June 28, 1999
Communicated by Stephen Wiggins

Summary. The nonlinear coupling of two scalar nonlinear Schrödinger (NLS) fields results in *nonfocusing* instabilities that exist independently of the well-known modulational instability of the *focusing* NLS equation. The focusing versus defocusing behavior of *scalar* NLS fields is a well-known model for the corresponding behavior of pulse transmission in optical fibers in the anomalous (focusing) versus normal (defocusing) dispersion regime [19], [20]. For fibers with birefringence (induced by an asymmetry in the cross section), the scalar NLS fields for two orthogonal polarization modes couple nonlinearly [26]. Experiments by Rothenberg [32], [33] have demonstrated a new type of modulational instability in a birefringent *normal* dispersion fiber, and he proposes this cross-phase coupling instability as a mechanism for the generation of ultrafast, terahertz optical oscillations. In this paper the nonfocusing plane wave instability in an integrable coupled nonlinear Schrödinger (CNLS) partial differential equation system is contrasted with the focusing instability from two perspectives: traditional linearized stability analysis and integrable methods based on periodic inverse spectral theory. The latter approach is a crucial first step toward a *nonlinear*, *nonlocal* understanding of this new optical instability analogous to that developed for the focusing modulational instability of the sine-Gordon equations by Ercolani, Forest, and McLaughlin [13], [14], [15], [17] and the scalar NLS equation by Tracy, Chen, and Lee [36], [37], Forest and Lee [18], and McLaughlin, Li, and Overman [23], [24].

MSC numbers. 35Q55, 58F07

* Funded in part by NSF DMS 97-04549.

† Funded by AFOSR F49620-98-1-0256 and NSF DMS 9600128.

‡ Supported by NSF DMR-9704724, DOE DE-FG02-88ER25053, and the Alfred P. Sloan Foundation.

§ Corresponding author, fax number 919-962-9345; e-mail: wright@amath.unc.edu.

PAC numbers. 02.30.Jr, 42.65.Sf

Key words. Defocusing instabilities, homoclinic orbits, coupling instabilities, integrable pdes, birefringent fibers

Introduction

The nonlinear Schrödinger (NLS) equation arises naturally as an envelope equation in physical wave systems where the propagation is governed by an asymptotic balance between the effects of dispersion and nonlinearity [29]. In nonlinear optics, the NLS describes the propagation of light pulses in a single-mode, nonlinear optical fiber [19]. Because of the polarized nature of light, fibers having near-axisymmetric cross-section can support two orthogonal co-propagating modes which are coupled through the fiber asymmetry. The evolution of the optical fields is described by a pair of coupled NLS-type equations [5], [6], [10], [26].

These coupled NLS (CNLS) systems are well-known to possess modulational instabilities, experimentally [32, 33] and theoretically [11], [31]. This optical instability is usually associated with anomalous dispersion fibers and the focusing scalar NLS equation; less well-known and far less understood is a coupling instability specific to the two-component birefringent fibers. Benney and Yang [42], [43] have studied the weakly oscillatory structures that arise from energy sharing between the two-component polarizations in the nonintegrable focusing and mixed focusing-defocusing cases with solitary wave initial conditions. The understanding of the cross-coupling instability of plane waves is the primary objective of our current investigations. In particular, this new instability is indeed an integrable phenomenon (just like the scalar focusing effect), and it persists in the purely *defocusing* equations even though the usual Benjamin–Feir mechanism of the focusing equations is absent. Moreover, the integrable structure of the equations implies that powerful tools may be available to explore the instability and what types of waveforms one can expect to result from it.

The integrability of the CNLS system under consideration means that there is an associated pair of linear operators (called a Lax pair of linear operators), one in time (t) and the other in space (x), in which the solutions of the CNLS system appear as coefficients. Compatibility of the two linear flows (i.e., the existence of simultaneous eigenfunctions $\vec{\psi}(x,t)$ such that $\vec{\psi}_{xt} = \vec{\psi}_{tx}$) is equivalent to the nonlinear evolution of the potentials according to the CNLS system. For the simplest class of constant-amplitude coupled NLS plane waves, the basic spectral elements of the associated linear problem, now with periodic plane wave coefficients, are explicitly constructed. In addition to the remarkable fact that the eigenmodes of the linearized CNLS system can be constructed from certain eigenfunctions of the Lax pair, these same Lax pair eigenfunctions can be used to construct the nonlocal behavior of the instability via a Bäcklund transformation [35]. In particular we provide a spectral criterion for modulational instability of a spatially periodic solution of the coupled NLS pdes, generalizing the corresponding results of Ercolani, Forest, and McLaughlin [13], [14], [15], [17] and Forest and Lee [18] for scalar integrable pdes. Once this behavior is revealed in the simple context of plane wave solutions, one can then exploit integrable pde tools to reveal information far be-

yond traditional linearized analysis. For the scalar integrable pdes with modulational instabilities (such as the focusing NLS and sine-Gordon equations), one now can give, from the results of Ercolani, Forest, and McLaughlin:

- spectral theoretic criteria for which solutions may be modulationally unstable,
- which spatial modes the wavetrain is unstable to,
- the growth-rate in each unstable mode,
- the dimension of the unstable manifold,
- a global parametrization of the unstable manifold,
- and an identification of which nonlinear wavetrains may saturate the instability.

Such information is clearly valuable in applications such as nonlinear birefringent optics, for example in understanding the apparent terahertz oscillations that saturate the modulational instability of defocusing fibers. One would like to both predict the instability of the initial data and then predict the saturated state and its frequency structure. To leading order, these are integrable properties. The evolution of the saturated states in the physical experiments are then governed by nearly integrable dynamics, which is accessible by perturbation methods.

The fact that coupled systems of NLS pdes may be integrable was shown by Manakov [25]. He exhibited systems of $(n + 1)$ NLS pdes which are formally completely integrable. The associated Lax pairs consist of linear matrix operators of order n, so-called higher order AKNS operators since they generalize the second-order AKNS (Ablowitz, Kaup, Newell, and Segur [1]) eigenvalue problems associated to KdV, sine-Gordon, focusing and defocusing NLS, and modified KdV equations. Manakov [25] calculated N-soliton solutions and provided much of the inverse scattering solution for coupled NLS equations with infinite-line boundary conditions. Beals, Deift and Tomei [7] developed scattering theory for general order n linear matrix operators, and Sattinger and Zurkowski [34] developed Bäcklund transformations for the pdes which arise as compatibility conditions for the Lax operator pairs.

Some of the inverse spectral theory relevant for periodic and quasiperiodic boundary conditions of the CNLS has been developed by Adams, Harnad, Hurtibise, and Previato [2], [3], [4]. For example, they obtained explicit formulas for a class of N-phase waves for the coupled NLS equations, the periodic analog of N-solitons, that could be coordinatized using the techniques of Moser [28]. McKean [22] and Previato [30] have also obtained results for the third-order scalar linear operator associated to the integrable Boussinesq pde under periodic boundary conditions. One of us has used several of the results developed in the present paper to address specific questions about the modulation equations for quasiperiodic CNLS plane wave solutions [40]. This paper uses the inverse spectral theory for the third-order AKNS linear operators associated to the coupled NLS pdes to identify the nonlocal structure of the simplest instabilities. Although Adams, Harnad, and Hurtibise [3], [4] derived explicit theta function formulae for certain multiphase solutions of the CNLS equations, the question of how these wavetrains are connected to instabilities in the equations was not addressed. In the case of unstable plane waves, we show that certain *stationary equations* of the hierarchy of flows commuting with the CNLS equations can be used to capture the low dimensional nonlocal behavior associated with the linearized instabilities of some unstable plane waves.

These orbits are near homoclinic orbits that can be explicitly constructed by Bäcklund transformations [12], [35].

Moreover, a fact that we wish to exploit is that *these additional cross-coupling instabilities exist in the integrable CNLS pdes independently of the focusing instability in the individual scalar pdes*. By developing methods of periodic inverse spectral theory for these special integrable cases, the nonlocal character of the instability can be studied, leading to a detailed understanding analogous to that already available for the scalar NLS equation. Understanding of the integrable system can then provide a basis for the understanding of more general, nonintegrable coupled evolutions, e.g. Yang and Benney [42], [43].

The simplest solutions of the NLS are *plane waves*: constant-amplitude exponential waves whose dispersion relations are amplitude-dependent. In the scalar NLS equations, there are two distinct cases: the defocusing case, in which the plane wave is stable, and the focusing case, in which a long wave modulational instability is present. This dichotomy has fundamental consequences in fiber optics: Plane wave stability allows for the transmission of continuous-wave laser light at wavelengths which lie in the normal dispersion regime (defocusing), whereas in the case of anomalous dispersion (focusing fibers) plane wave instability saturates in the formation of envelope solitons which then propagate as stable pulses. This was the scenario laid out in the early 1970s by Hasegawa and Tappert [21], and the investigations since have centered around the various higher order perturbative terms that couple to the integrable NLS evolution and which affect soliton pulse propagation. We refer to the recent book by Hasegawa and Kodama [20] for a thorough treatment of fiber optics and scalar NLS equations, both integrable and perturbed. Furthermore, optical fibers in use today employ "super-Gaussian" pulses as normal modes of propagation (in spite of the fact that the fibers support stable soliton pulses), thus making the study of the nonlinear phenomena arising from instabilities in the equations an important applied field.

The coupled NLS system, focusing or defocusing, also possesses a two-component analog of plane wave solutions. Laboratory and numerical experiments [33] have observed modulational instability in optical fibers with defocusing dispersion. The striking feature of these experiments is that the phenomenon of modulational instability and saturation into localized pulse-like shapes was previously associated only with focusing fibers. An understanding of why this phenomenon appears in defocusing fibers is clearly important. As we show below, this phenomenon exists in the integrable defocusing CNLS equations, and occurs through a cross-coupling instability that is independent of stability within the individual uncoupled modes. We cannot claim that we are making the first observation of the integrable basis of this phenomenon; Forest and a collaborator, Daniel David, noted this fact about ten years ago and surely others have made the connection. We are, however, pursuing its mathematical consequences by using and developing methods of integrable soliton theory.

With respect to the integrable description of the linearized instability of CNLS pdes, we present the analogous elements of the scalar theory:

- the fundamental elements of the periodic spectral theory associated to the CNLS equations,
- specific results for instabilities of constant-amplitude plane waves,

- a prescriptive theory for the link between the linearized stability theory and the inverse spectral theory,
- an explicit construction, using the inverse theory, of the low dimensional nonlocal waveforms (homoclinic orbits) and some of the nearby quasiperiodic orbits which characterize the phase space of the integrable system when the plane waves are perturbed by unstable modes of the linearized equation.
- an explicit construction of the finite dimensional system of odes that governs the evolution of a simple class of multiphase solutions near the homoclinic orbits of defocusing CNLS plane waves.

The complete characterization of the constraints which the initial data must satisfy in order to obtain a global solution in terms of theta functions remains an open problem.

The Basic Equations

The integrable generalization of the NLS equation to a two-component system is obtained by straightforward vectorization of the scalar NLS evolution

$$i\,\vec{r}_t + \vec{r}_{xx} + \frac{\sigma}{2}|\vec{r}\,|^2\,\vec{r} = 0, \tag{1}$$

where t, x are time and space coordinates. Note, however, that in the context of fiber optics the roles of t and x are reversed. Denoting the two components of the vector $\vec{r}$ by complex-valued scalar fields $p(x,t)$ and $q(x,t)$, the evolution can be written as the coupled PDE system,

$$\begin{aligned} i\,p_t + p_{xx} + \tfrac{\sigma}{2}(|p|^2 + |q|^2)\,p = 0, \\ i\,q_t + q_{xx} + \tfrac{\sigma}{2}(|p|^2 + |q|^2)\,q = 0, \end{aligned} \tag{2}$$

where the nonlinearity appears through the sum of the squared magnitudes of the components of $\vec{r}$.

In both the scalar and vector cases, the sign of the nonlinearity distinguishes two evolutions and two types of fiber regimes: $\sigma = +1$ corresponds to focusing behavior and anomalous dispersion fibers, while $\sigma = -1$ corresponds to defocusing behavior and normal dispersion fibers. The coupled system will be shown to possess an additional instability that occurs even with the defocusing nonlinearity, i.e., an instability due to the nonlinear coupling.

There is also a third integrable form where the nonlinearity appears as the difference of the squared magnitudes of the components — this results in a hybrid coupling whereby one component defocuses while the other focuses. This case will not be considered here.

Plane Wave Solutions

The simplest exact solution to the coupled NLS equations is the *plane wave* — a constant-amplitude, exponential wavetrain,

$$p_o = a e^{i(+kx-\omega t)}, \qquad q_o = b e^{i(-kx-\omega t)}, \tag{3}$$

whose frequency ω is required to satisfy the amplitude-dependent dispersion relation,

$$\omega = k^2 - \frac{\sigma}{2}(|a|^2 + |b|^2) = k^2 - \frac{\sigma}{2} I^2, \tag{4}$$

where $I^2 \equiv |a|^2 + |b|^2$ gives the total intensity of the plane wave. The complex amplitudes a, b are constants, thereby defining a wave having fixed *polarization* — that is, a wave where the division of intensity between the two components p and q is uniform in both time and space.

In the above representation of the plane wave, the wavenumbers for each component are assumed real and have opposite signs. This antisymmetry is imposed without loss of generality, since a symmetric shift in wavenumber can be compensated by a suitable adjustment in the phase velocity (ignoring spatial boundary conditions). This feature of the plane wave solution results from the more general Galilean invariance property possessed by both the NLS and its coupled version, and can be considered as merely a transformation to moving coordinates,

$$\vec{r}(x,t) \to \vec{r}(x - 2\gamma t, t)\, e^{i\gamma(x-\gamma t)}, \tag{5}$$

where γ is an arbitrary real parameter representing the half-velocity of the new reference frame. For the plane wave, this is also seen to be equivalent to a symmetric shift of γ in the wavenumbers.

There is an additional symmetry which is particular to the coupled NLS equations, which in the language of symmetry groups is equivalent to an SU(2) symmetry. This essentially means that the solution set is invariant under both rotations of the p, q coordinate basis for the field vector $\vec{r}$ and arbitrary complex phase shifts. Explicitly, any solution transforms to another solution upon multiplication by the 2×2 unitary matrix

$$\vec{r}(x,t) \to \begin{bmatrix} \cos\theta\, e^{+i\phi} & -\sin\theta\, e^{+i\phi} \\ \sin\theta\, e^{-i\phi} & \cos\theta\, e^{-i\phi} \end{bmatrix} \vec{r}(x,t), \tag{6}$$

where θ can be thought of as a rotation of polarization in the p, q coordinate axes and ϕ some asymmetric complex phase shift. The rotational nature of this transformation provides the simplest means for generating coupled NLS waves from known scalar solutions [11].

Plane Wave Stability Analysis

The linearized stability of the plane wave is easily obtained from Fourier analysis. It proves most convenient to introduce the disturbance quantities $\tilde{p}(x,t)$ and $\tilde{q}(x,t)$ as multiplicative perturbations to the plane wave

$$p = p_o(1 + \tilde{p}), \qquad q = q_o(1 + \tilde{q}), \tag{7}$$

since this results in a convenient simplification upon linearization. Keeping only terms linear in $\tilde{p}, \tilde{q}$ after direct substitution of (7) into the coupled NLS equations (2), the

linearized disturbance equations become

$$\begin{aligned} i\,(\tilde{p}_t + 2k\tilde{p}_x) + \tilde{p}_{xx} + \tfrac{\sigma}{2}|a|^2(\tilde{p}+\tilde{p}^*) + \tfrac{\sigma}{2}|b|^2(\tilde{q}+\tilde{q}^*) = 0, \\ i\,(\tilde{q}_t - 2k\tilde{q}_x) + \tilde{q}_{xx} + \tfrac{\sigma}{2}|a|^2(\tilde{p}+\tilde{p}^*) + \tfrac{\sigma}{2}|b|^2(\tilde{q}+\tilde{q}^*) = 0, \end{aligned} \tag{8}$$

where the superscript * denotes complex conjugation.

Because of the conjugates in (8), the eigenfunctions are most conveniently expressed as linear combinations of pure Fourier modes,

$$\begin{aligned} \tilde{p} &= f_+ e^{i\kappa(x-\Omega t)} + f_-^* e^{-i\kappa(x-\Omega^* t)}, \\ \tilde{q} &= g_+ e^{i\kappa(x-\Omega t)} + g_-^* e^{-i\kappa(x-\Omega^* t)}. \end{aligned} \tag{9}$$

These eigenmodes are parameterized by the real wavenumber κ of the disturbance and the complex phase velocity Ω, where a positive imaginary part indicates a pure temporal growth mode of instability in positive time. Substitution into the linearized pdes (8) and collection of resonant terms results in four linear homogeneous equations for the Fourier amplitudes $f_\pm$ and $g_\pm$,

$$\begin{aligned} (+\Omega - 2k - \kappa)\kappa\ f_+ + \tfrac{\sigma}{2}|a|^2\,(f_+ + f_-) + \tfrac{\sigma}{2}|b|^2\,(g_+ + g_-) = 0, \\ (-\Omega + 2k - \kappa)\kappa\ f_- + \tfrac{\sigma}{2}|a|^2\,(f_+ + f_-) + \tfrac{\sigma}{2}|b|^2\,(g_+ + g_-) = 0, \\ (+\Omega + 2k - \kappa)\kappa\ g_+ + \tfrac{\sigma}{2}|a|^2\,(f_+ + f_-) + \tfrac{\sigma}{2}|b|^2\,(g_+ + g_-) = 0, \\ (-\Omega - 2k - \kappa)\kappa\ g_- + \tfrac{\sigma}{2}|a|^2\,(f_+ + f_-) + \tfrac{\sigma}{2}|b|^2\,(g_+ + g_-) = 0. \end{aligned} \tag{10}$$

Solvability for this system requires that the determinant of the matrix of coefficients vanish — this determines the *dispersion relation for linearized disturbances*

$$\left[(\Omega - 2k)^2 + (\sigma|a|^2 - \kappa^2)\right]\left[(\Omega + 2k)^2 + (\sigma|b|^2 - \kappa^2)\right] - |a|^2|b|^2 = 0, \tag{11}$$

yielding a quartic polynomial for the complex frequency $\Omega(\kappa)$ in terms of the disturbance wavenumbers $\kappa > 0$ and the plane wave parameters; if $\kappa = 0$ then the determinant of the matrix of coefficients is identically zero, so this factor has been removed from the dispersion relation.

For real wavenumbers κ, the polynomial has real coefficients and therefore, complex roots Ω occur in conjugate pairs. Those roots with nonzero imaginary part correspond to linearly unstable modes, with growth rate $|\mathrm{Im}(\Omega(\kappa))|$. Furthermore the polynomial only contains κ^2, which reflects the conjugate symmetry of the eigenmodes, so it is sufficient to consider only $\kappa \geq 0$. Note also that the case $\kappa = 0$ is degenerate and is treated separately in the later section when the issue of completeness of the set of linearized eigenfunctions is addressed.

Since this polynomial defies direct factorization, the analysis of this linearized dispersion relation is performed in various asymptotic limits and the results assembled to construct a complete stability picture for the plane wave.

Short-Wave Stability

In the stability analysis for the scalar NLS, the behavior of high-wavenumber eigenmodes is dominated by the derivative terms of the linearized wave operator so that

plane waves are found to be neutrally stable to all disturbances having sufficiently short wavelength. This behavior is no different in the coupled system, where in the limit of large-wavenumber disturbances ($\kappa \gg k, |a|^2, |b|^2$), the four roots Ω can be found asymptotically

$$\Omega \sim \pm\kappa \pm 2k + O(\kappa^{-1}), \tag{12}$$

so that all phase velocities Ω are clearly real and distinct to leading order. Since complex roots can only occur as complex conjugates (having equal real parts), all higher order corrections are necessarily real, thus implying neutral stability of the plane wave to all short-wavelength disturbances. Since this result is independent of the sign of σ, it applies equally to both the defocusing and focusing systems.

Long-Wave Instability

For disturbances having precisely zero-wavenumber, the dispersion relation is trivially satisfied for all values of Ω, so that the possibility exists for complex eigenvalues to arise in the breaking of this quadruple-zero degeneracy at small, but nonzero κ. As expected, the focusing nonlinearity leads to long-wave instability consistent with the classical Benjamin-Feir [9] long-wave instability of the focusing NLS.

At small, nonzero wavenumbers ($\kappa \ll k, |a|^2, |b|^2$), the eigenvalues Ω for long-wave disturbances are determined by the leading order stability polynomial

$$(\Omega^2 - 4k^2)^2 + \sigma|a|^2(\Omega + 2k)^2 + \sigma|b|^2(\Omega - 2k)^2 = O(\kappa^2). \tag{13}$$

Immediately it is clear that, with the choice of $\sigma = +1$, this leading order part is positive definite and all roots Ω must be complex. This confirms the expected result that *the coupled NLS demonstrates a focusing instability in the limit of zero-wavenumber disturbances*.

For σ negative, i.e. the defocusing case, the leading order polynomial is indefinite, and the stability picture depends critically on the parameters of the underlying plane wave — in particular, on the comparative magnitudes of its wavenumber k and amplitudes $|a|^2, |b|^2$. The stability character of the roots is easily inferred asymptotically in the extremes where either parameter is relatively small.

At small amplitudes, the quartic terms in the polynomial (13) dominate. For ($\kappa \ll |a|^2, |b|^2 \ll k$), all four phase velocities are found to be real and distinct to leading order

$$\Omega \sim \begin{cases} +2k \pm \sqrt{|a|^2}, \\ -2k \pm \sqrt{|b|^2}, \end{cases} \tag{14}$$

so that these plane waves are thus stable to long-wave disturbances. On the other hand, in the opposite limit of relatively large amplitudes ($\kappa \ll k \ll |a|^2, |b|^2$), two of the roots are obtained by neglecting the quartic terms in (13) and determined to leading order by the remaining quadratic terms

$$|a|^2\,(\Omega + 2k)^2 + |b|^2\,(\Omega - 2k)^2 = O(k^4, \kappa^2), \tag{15}$$

which are positive definite and confirm the existence of at least two complex phase velocities Ω. In summary then, these asymptotic results verify that unlike the one-component NLS, *the coupled NLS can exhibit long-wave instabilities even with the choice of defocusing nonlinearity*.

However, we show next that the mechanism by which this instability occurs is quite distinct from the usual focusing behavior.

Cross-Phase Resonance

Defocusing Equations

The first hint of an essential difference in the nature of the defocusing instability is the observation that plane waves are stabilized in the limit when the spatial modulation is absent ($k = 0$)

$$\Omega = \begin{cases} \pm\kappa \\ \pm\sqrt{\kappa^2 + |a|^2 + |b|^2} \end{cases}, \tag{16}$$

yet there is instability when k is small and nonzero (15). By analyzing the marginally stable normal modes, it is found that there is a band of unstable disturbance wavenumbers κ that scales linearly with the carrier wavenumber k according to $\kappa \approx \pm 2k$. The defocusing instability occurs when two plane waves with different wavenumbers are present, and thus is clearly seen to be intrinsically linked to the coupled nature of the equations.

Since complex eigenvalues occur in conjugate pairs, the marginal stability condition (corresponding to a change in stability) coincides with the conditions for the dispersion relation (11) to have a real double-root. The vanishing of the *resultant* between the stability polynomial (11) and its Ω-derivative provides a necessary criterion for this double-root. Analysis of this polynomial condition allows for the determination of the boundary between regions of stability and instability in the space of parameters $k, \kappa, |a|^2, |b|^2$.

The resultant simplifies greatly in the special case of a plane wave having equal intensities in both components, viz. $|a|^2 = |b|^2$, and the band of unstable normal modes is given by

$$4k^2 - I^2 < \kappa^2 < 4k^2, \tag{17}$$

where $I^2 = |a|^2 + |b|^2 = 2|a|^2$ represents the total intensity of the plane wave. The region of instability is thus bounded by a hyperbola and its asymptotes. These are shown by solid curves in Figure 1, where the wavenumbers κ and k have been normalized on the amplitude $|a|$. As the division of intensity becomes more unequal, the κ-bandwidth of the unstable modes shrinks, while the shape of the marginal stability boundaries remains qualitatively similar, as in Figure 2 (solid curves). At the single polarization limit, where all of the wave intensity is concentrated in just one component, the marginal curves collapse onto each other at the limiting curve (with $\sigma = -1$),

$$\kappa = \pm\frac{16k^2 + \sigma|a|^2}{8k}, \tag{18}$$

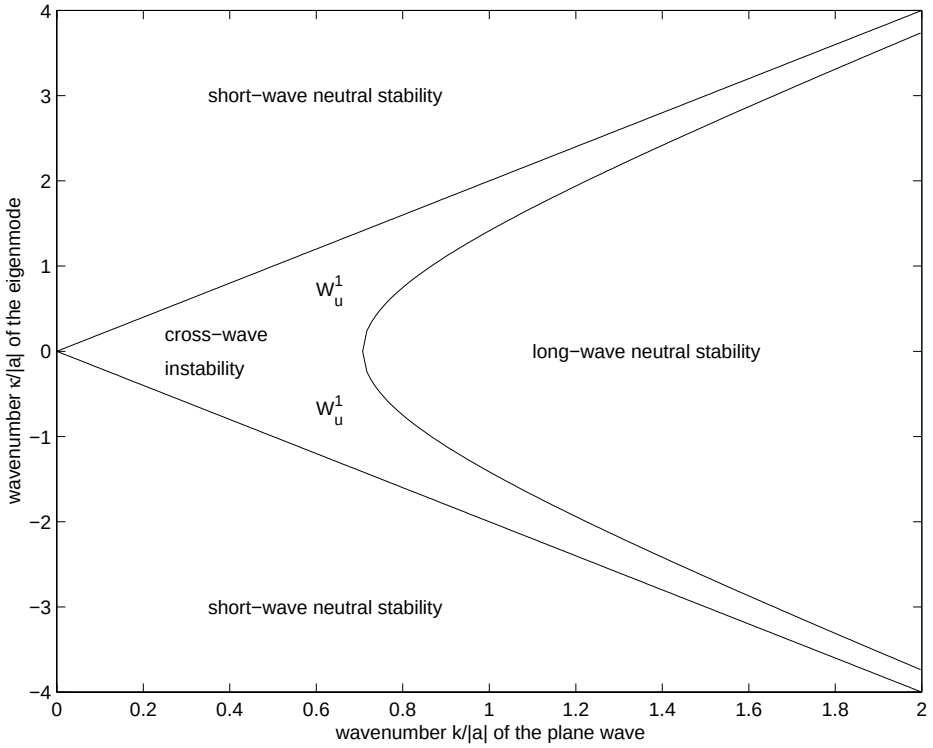

Fig. 1. Marginal stability curves for the defocusing equations with equal intensity plane waves ($|a| = |b|$). The dimension of W_u^1, the unstable manifold corresponding to each wavenumber in the unstable sidebands, is one. The cross-phase sideband resonance for the defocusing instability of plane waves is, in general, at *intermediate* wavelengths. See Figure 2 for the marginal stability curves in the case of unequal division of intensity between the two channels.

for $k \geq \frac{1}{4}|a|$, and the horizontal axis for $0 \leq k \leq \frac{1}{4}|a|$, which appear as the dashed curves in Figure 2.

Focusing Equations

The corresponding analysis for the focusing case reveals that plane waves are subject to both self-phase focusing instabilities and cross-phase coupling instabilities. The marginal stability curves in wavenumber-space are shown in Figure 3 for the case of equal amplitudes in each polarization. Figure 4 shows the marginal stability curves for unequal intensities, and Figure 5 shows the collapse of the sidebands in the self-phase single polarization limit, reproducing the classical Benjamin-Feir instability band $0 < (\frac{\kappa}{|a|})^2 < 1$.

The *dimension* of the unstable manifold and the *qualitative* nature of the instability varies as the wavenumber parameters move throughout the unstable region. The dimension of the unstable manifold corresponding to a given wavenumber is found from the eigenmode basis of the linearized equation. The *nonlocal* qualitative nature of the instabilities is revealed by the global construction of the corresponding homoclinic orbit using a Bäcklund transformation. Note that the Bäcklund transformation used to ob-

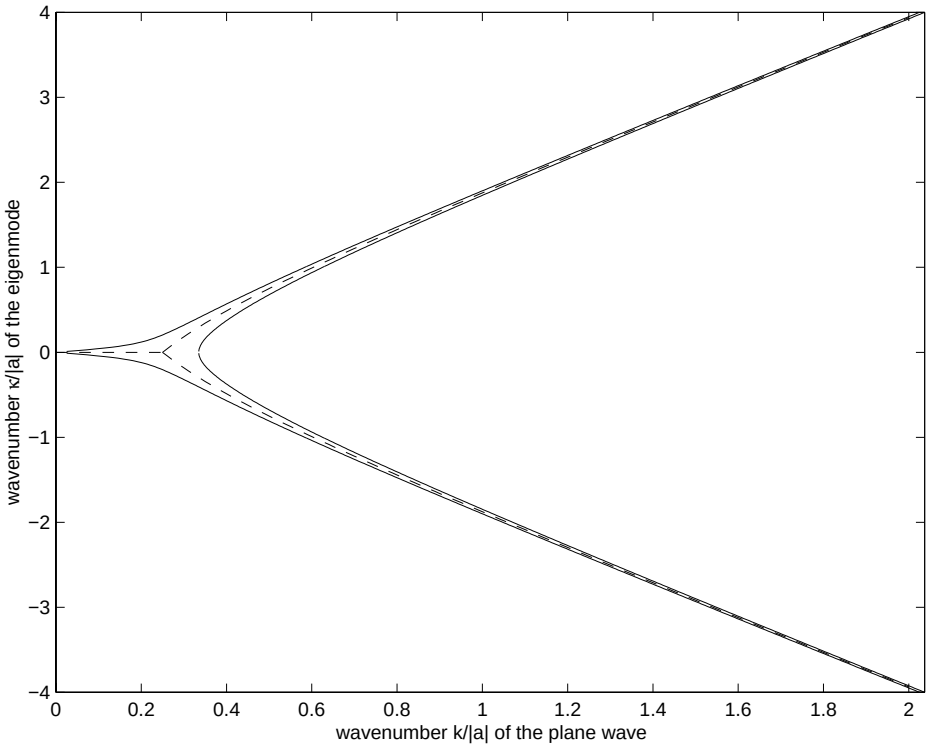

Fig. 2. Marginal stability curves (solid lines) for the defocusing instability of plane waves in a case of intermediate division of intensity between the two channels, viz. $|a|^2 = 100|b|^2$. In the single polarization limit ($|b| \to 0$) the marginal stability curves collapse upon themselves at the limiting curves indicated by the dashed curves and the unstable region vanishes, as expected for the scalar defocusing NLS equation. Compare with Figure 1 which shows the marginal stability curves for coupled plane waves with equal intensities.

tain the correct homoclinic orbit depends on the one-to-one correspondence between the eigenmodes for each wavenumber (for both $\kappa \geq 0$ and $\kappa \leq 0$ separately) and the Floquet spectral points to be discussed in the integrable theory of the following sections.

In order to explain the instability diagrams of Figure 3 and Figure 4, two types of nonlocal behavior generated by individual eigenmodes must be distinguished:

- *Cross-phase* instabilities, where the maximum magnitude of the disturbance generated by the unstable eigenmode is the same in the two channels. Qualitatively, there is an equal excitation of each channel by the instability. The energy is shared by the two co-propagating channels.
- *Self-phase* instabilities, where the maximum magnitude of the disturbance generated by the unstable eigenmode is larger in one channel than in the other channel. Qualitatively, the disturbance is greater in one channel than in the other channel. The instability mode is primarily associated with one channel, although there is some sharing of energy as dictated by the relative intensity distribution of the background plane wave.

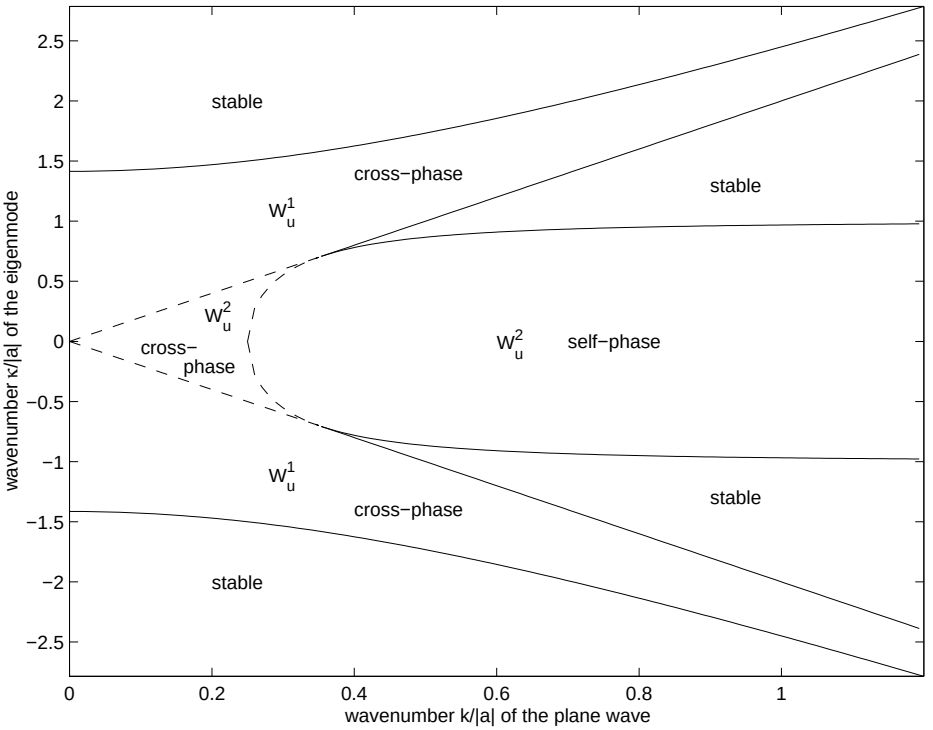

Fig. 3. Marginal stability curves (solid curves) for the focusing instability of plane waves with equal intensities ($|a| = |b|$). Three distinct regions of instability can be identified in the unstable wavenumber region: cross-phase sidebands with one unstable mode denoted by W_u^1 cross-phase, a cross-phase transition region with two unstable modes denoted by W_u^2 cross-phase, and a central self-phase band of two unstable modes denoted by W_u^2 self-phase. These regions of instability are separated by dashed lines.

Focusing Case: Equal Division of Intensity

In the case of equal division of intensity in the two channels ($|a| = |b|$), Figure 3 can be divided into three distinct regions of instability:

- *Cross-phase* W_u^1*:* The unstable manifold is a cross-phase instability of dimension one.
- *Cross-phase* W_u^2*:* The unstable manifold is a cross-phase instability of dimension two. Both unstable eigenmodes generate cross-phase disturbances. As the wave parameters cross the boundary from W_u^1 to W_u^2 cross-phase, the original short-wave cross-phase disturbance is preserved but a new long-wave cross-phase instability is generated with large spatial structure. As the wave parameters move toward the boundary with the W_u^2 self-phase region, the scales of the disturbances generated by the two unstable cross-phase modes become comparable.
- *Self-phase* W_u^2*:* The unstable manifold is a self-phase instability of dimension two. Both unstable eigenmodes generate self-phase disturbances. One eigenmode excites the p-channel more than the q-channel, while the other excites the q-channel more than the p-channel. The self-phase nature of each instability becomes less pronounced

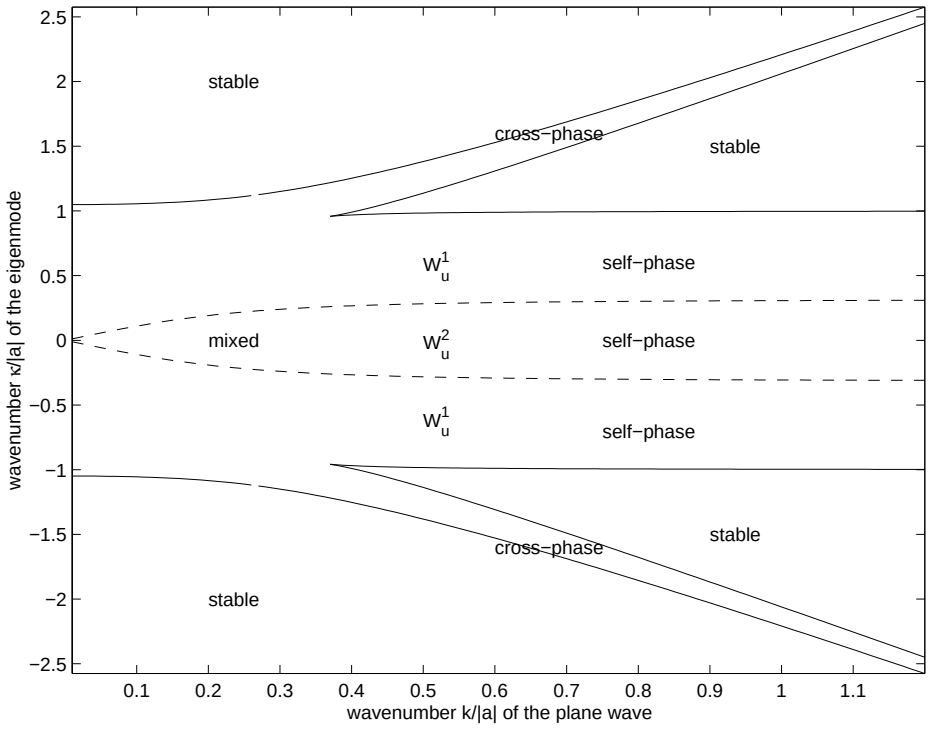

Fig. 4. Marginal stability curves for the focusing instability of plane waves (solid lines) in the case of intermediate division of intensity between the two channels, viz. $|a|^2 = 10|b|^2$. Region W_u^1 is a region of one-dimensional instability. There is a continuous cross-phase/self-phase deformation in the nonlocal structure as the wave parameters move from the sidebands (cross-phase) to the horizontal band (self-phase). The narrow horizontal band denoted by W_u^2 is a region of two-dimensional instability. Both instabilities are self-phase in nature for large $\frac{k}{|a|}$ but one of them becomes mixed with cross-phase properties as the normalized wavenumber decreases.

near the boundary with the W_u^2 cross-phase region, and becomes more pronounced as $\frac{k}{|a|} \to \infty$.

It is worth emphasizing that the qualitative nonlocal structure of the instabilities varies *continuously* as the wave parameters vary continuously within the unstable region.

Focusing Case: Unequal Division of Intensity

In the case of unequal division of intensity in the two channels, where the p-channel is ten times stronger than the q-channel ($|a|^2 = 10|b|^2$), Figure 4 can be divided into two regions of instability denoted by W_u^1 and W_u^2 according to the dimension of the unstable manifold. Each of these regions also exhibits subregions in which the qualitative nature of the nonlocal structure is different:

- *Cross-phase* W_u^1, where the unstable manifold is a (relative) cross-phase instability of dimension one in which both channels exhibit significant growth, although the relative

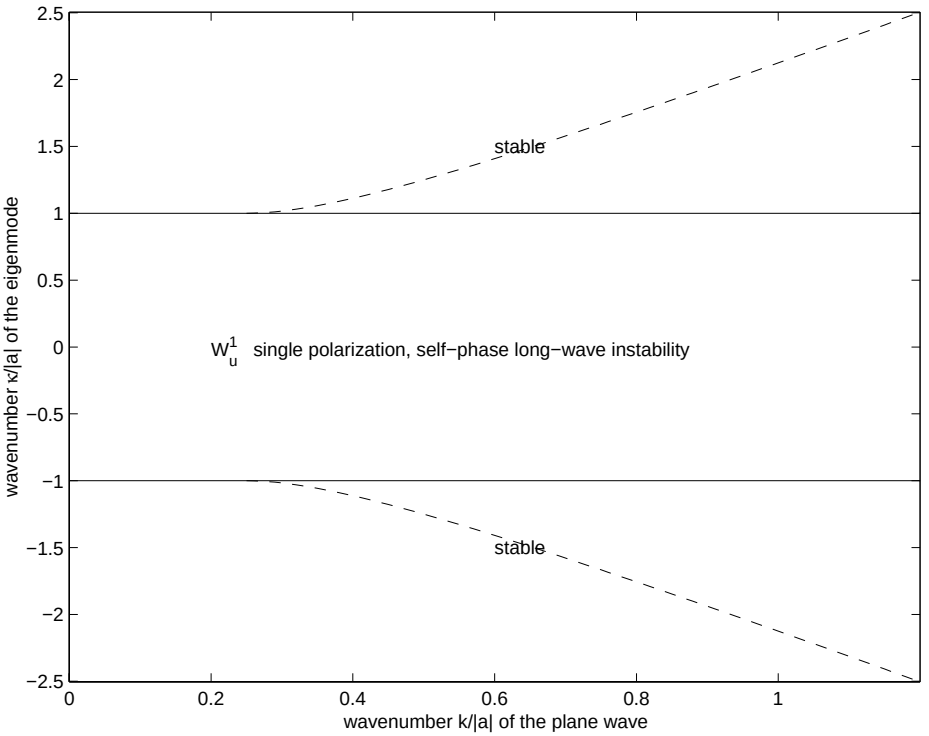

Fig. 5. In the single polarization limit ($|b| = 0$), the cross-phase sidebands of the focusing instability diagrams collapse onto the dashed curve, leaving a horizontal band (solid curve) of pure one-dimensional long-wave focusing instabilities described by the simple classical condition $0 < \frac{k^2}{|a|^2} < 1$. A narrow band of two-dimensional self-phase instabilities has collapsed along the horizontal axis.

dominance of the p-channel is inherited from the fundamental wave. These regions appear as two sidebands in the instability diagram.

- *Self-phase* W_u^1, where the unstable manifold is a self-phase instability of dimension one. There is a continuous deformation of the nonlocal structure as the wave parameters move from the cross-phase sidebands to the central self-phase band of W_u^1 through a transition region. This deformation is observed as a continuous strengthening of the disturbance in the p-channel and weakening of the disturbance in the q-channel, until the instability hardly excites the q-channel at all in the self-phase band.
- *Self-phase* W_u^2, where the unstable manifold is of dimension two, one unstable mode excites the p-channel almost exclusively, while the other unstable mode excites the q-channel almost exclusively. This region appears as a narrow central band in the instability diagram.
- *Mixed* W_u^2, where the unstable manifold is of dimension two. One instability is relatively unchanged from the long-wave self-phase mode that excites the q-channel in the self-phase W_u^2 region. The second instability is a continuous deformation of the structure that appears in the transition region between the cross-phase and self-phase

W_u^1 regions. Although the p-channel is still larger in absolute magnitude, significant energy is transferred to the q-channel. At the same time the features of the disturbance become smaller in scale. This second mode is the one which is preserved when the dimension of the unstable manifold drops to one in the region W_u^1.

A number of remarks can be made about the two cases. In both Figures 3 and 4 there are cross-phase instabilities in a sideband of intermediate wavenumbers bordered by an hyperbola and asymptotes having slope $\sim \pm 2k$. In the case of equal intensities, Figure 3, the transition from one-dimensional cross-phase behavior to two-dimensional self-phase behavior occurs through a transitional two-dimensional cross-phase region. This is due to the fact that neither channel is preferentially chosen by the fundamental plane wave whose intensity is equally distributed between the two channels. When one channel is preferentially selected by the fundamental plane wave as in Figure 4, where the intensities are unequal in the unperturbed plane wave, a continuous deformation from one-dimensional (relative) cross-phase behavior to one-dimensional self-phase behavior can occur while one channel remains dominant in absolute terms. In the single polarization limit, Figure 5 shows that the self-phase region W_u^1 from Figure 4 remains and that the central W_u^2 region has collapsed and vanished on the horizontal axis, while the cross-phase sidebands have collapsed and vanished on the curve given by Equation (18), with $\sigma = +1$. The remaining horizontal band of long-wave instabilities is precisely the instability diagram for the scalar focusing NLS equation.

Note also that in the regions where two-dimensional self-phase instabilities exist, the two instabilities could be combined to produce a type of mixed self-phase and cross-phase behavior.

In general, the conditions at which plane waves are marginally stable to the cross-phase instability can be ascertained asymptotically for large plane wavenumber k

$$\kappa^2 \sim 4k^2 + \frac{\sigma}{4}(\sqrt{|a|^2} \pm \sqrt{|b|^2})^2 + \frac{(|a|^2 - |b|^2)^2}{64k^2}, \tag{19}$$

a result consistent with the two previous exact cases of equal and singly polarized limits (17), (18). In particular, it is noted that the κ-bandwidth of the instability scales inversely with the linearized group velocity k, and suggests that the spatial structure of unstable envelope disturbances also has wavelengths that scale proportionally with k.

Completeness of the Eigenmode Basis

The eigenvector associated with an eigenvalue $\Omega(\kappa)$, for $\kappa > 0$, has the simple, implicit representation,

$$\begin{pmatrix} f_+ \\ f_- \\ g_+ \\ g_- \end{pmatrix} = \begin{pmatrix} (+\Omega - 2k - \kappa)^{-1} \\ (-\Omega + 2k - \kappa)^{-1} \\ (+\Omega + 2k - \kappa)^{-1} \\ (-\Omega - 2k - \kappa)^{-1} \end{pmatrix}, \tag{20}$$

and supplies the Fourier amplitudes that determine a linear eigenmode (9). Since the equivalent of two independent Fourier modes at each wavenumber is required to span

a complex field, a total of four eigenmodes are needed to complete the linearized basis for $\tilde{p}$ and $\tilde{q}$ over the real field. If, for a given κ, the four roots Ω of the polynomial (11) are distinct, then the set of eigenmodes generated by the above Fourier constants are spatially complete. The only exceptions to this simple state of affairs arise at the degenerate $\kappa = 0$ Fourier mode and the possibility of multiple-roots $\Omega(\kappa)$.

For $\kappa = 0$, the eigenvalue condition is degenerate since the complex fields are spatially uniform. By inspection of the linearized equations, three independent constant solutions are obtained:

$$\begin{pmatrix} \tilde{p} \\ \tilde{q} \end{pmatrix} = \begin{pmatrix} i \\ 0 \end{pmatrix}, \qquad \begin{pmatrix} 0 \\ i \end{pmatrix}, \qquad \begin{pmatrix} |b|^2 \\ -|a|^2 \end{pmatrix}. \tag{21}$$

Additional secular-in-t solutions can be obtained by the formal differentiation of the original plane wave by the parameters $|a|$ and $|b|$, remembering that ω also depends on these parameters via the dispersion relation. A symmetric sum of secular solutions is

$$\begin{pmatrix} \tilde{p} \\ \tilde{q} \end{pmatrix} = (i\,\sigma I^2 t + 1) \begin{pmatrix} 1 \\ 1 \end{pmatrix}. \tag{22}$$

Any *real* linear combination of these four solutions provides a complete basis of spatially-uniform disturbances.

These space-independent linearized modes are indicative of perturbations that are equivalent to infinitesimal changes in the parameters of the general plane wave (3). The three time-independent modes are a consequence of small shifts in the complex phases of either p_o or q_o, and changes in amplitudes $|a|^2$, $|b|^2$ which leave the total intensity I^2 fixed. The fourth mode corresponds to amplitude perturbations which change the total intensity, I^2 — the temporal secularity is a manifestation of a change in the frequency $\omega(I)$ as required by the plane wave dispersion relation (4).

An additional time-independent linearized mode arises at $\kappa = \pm 2k$ and corresponds to the rotational symmetry of the component fields (6).

For all other multiple-root degeneracies, formal differentiation by Ω of the eigenmode as determined by using equations (9), (20) produces additional temporally secular modes with which the linearized basis can be completed.

Note the following observations concerning the linear effect on $|p|^2$ and $|q|^2$ when the plane wave is perturbed by eigenmodes determined by equations (9), (11), (20):

- Since each eigenmode is arbitrary up to multiplication by a complex constant, the linearized dynamics of a spatial perturbation produced by an eigenmode is arbitrary up to a spatial phase shift in $|p|^2$ and $|q|^2$.
- Similarly, replacing κ by $-\kappa$ in the eigenmode also produces a phase shift in the spatial perturbation and, hence, is equivalent in the linearized dynamics to a spatial translation.
- If $Im(\Omega(\kappa)) > 0$, then the eigenmode is unstable in positive time and there is a corresponding asymptotically stable eigenmode with $Im(\Omega(\kappa)^*) < 0$. Replacing Ω by its complex conjugate in the eigenmode merely produces a phase shift in the spatial perturbation.

Integrable Theory

The previous linearized theory begins to explain the origin of two classes of instability, cross-phase and self-phase. To more fully understand the qualitative behavior of the system as the disturbances grow into large perturbations from the basic plane wave, it is necessary to assemble a less local picture of the nonlinear dynamics. In particular, it will be especially useful to discover if, and how, the unstable defocusing dynamics differs nonlocally from the focusing dynamics, which one might expect to have a greater similarity with scalar NLS behavior. Integrable theory can be used to obtain a nonlocal picture of the dynamics of the instability. The eigenmodes (for $\kappa \geq 0$ or for $\kappa \leq 0$) of the linearized equations will be seen to be in one-to-one correspondence with certain distinguished points in the spectrum of the Lax pair which integrates the CNLS system. This correspondence provides a simple geometric criterion for instability of the eigenmode: Unstable modes are associated with nonreal double points of the Floquet curve; stable modes are associated with real double points.[1] This correspondence is similar to the situation in the scalar NLS equation with the following important difference: In the case of the third-order Lax operator, the coincidence of periodic/antiperiodic eigenvalues and geometric double points is lost. A similar observation is made by McKean [22] in the case of the Boussinesq equation.

Once the correspondence has been established between the nonreal double points and the linearized instabilities, it is possible to use Bäcklund transformations to generate homoclinic orbits that result from the instability. Some results in this direction were obtained by Sheu [35], and here we will isolate some of the simplest cases to illustrate the difference between the focusing and nonfocusing unstable manifolds. Moreover, a function space neighbourhood of the finite-dimensional phase space near at least some of the homoclinic orbits can be found by using stationary equations of the integrable CNLS hierarchy [41]. This will demonstrate the presence of crossed homoclinic saddles in the phase space of the focusing and *defocusing* CNLS fields, similar to the structure described by Ercolani, et al. [15], [16], for the Sine-Gordon and the focusing scalar NLS equations. The phase-space geometry of such "whiskered tori"[2] is also discussed in McLaughlin and Overman [23].

The integrability of the coupled NLS system (2) is established by similar means as for the scalar NLS equation. Because of the two field components, the integrable theory for the coupled version is essentially a block-matrix generalization of the usual AKNS scheme. The crucial transformation from the complex fields $p(x,t)$ and $q(x,t)$ to a spectral representation is achieved through the third-order, linear ODE system,

$$\vec{\psi}_x = \begin{bmatrix} -\frac{2}{3}iE & \frac{1}{2}p & \frac{1}{2}q \\ -\frac{\sigma}{2}p^* & \frac{1}{3}iE & 0 \\ -\frac{\sigma}{2}q^* & 0 & \frac{1}{3}iE \end{bmatrix} \vec{\psi} \equiv \mathbf{L}\vec{\psi}, \tag{23}$$

[1] For data other than plane waves (not dealt with in this paper), there may be rare exceptional cases where the growth-rate associated with a nonreal double point vanishes.

[2] In our case the torus is given by the periodic plane wave and the whiskers are given by the homoclinic orbits that generate the unstable manifold.

which introduces E, the spectral eigenvalue. The inherent degeneracy of this operator follows from the equality of the eigenvalue contributions along the diagonal, so that the roles of p and q are interchangeable. As a consequence of this symmetry, the resulting spectral theory is quite distinct from that of the relevant third-order Lax operator pair for the three-wave resonant interaction equations [8]. The development of the degenerate, third-order spectral theory that follows is primarily motivated through analogy to the scalar NLS analysis where the extra order is handled by treating the lower-right 2×2 sub-matrix as a block element [7], [34].

Because of the additional complexity introduced by the third-order nature of the spectral operator, it proves expedient to stay within a matrix-based formulation. Two fundamental matrices are defined by decomposing the spectral operator $\mathbf{L}$ into an eigenfunction part and a scattering part,

$$\mathbf{L} = E\, A_0 + A_1, \tag{24}$$

so that A_0 is a constant diagonal matrix, and $A_1(x,t)$ is a scattering matrix containing both of the coupled complex fields $p(x,t)$ and $q(x,t)$. Explicitly,

$$A_0 = \begin{bmatrix} -\frac{2i}{3} & 0 & 0 \\ 0 & \frac{i}{3} & 0 \\ 0 & 0 & \frac{i}{3} \end{bmatrix}, \qquad A_1 = \begin{bmatrix} 0 & \frac{1}{2}p & \frac{1}{2}q \\ -\frac{\sigma}{2}p^* & 0 & 0 \\ -\frac{\sigma}{2}q^* & 0 & 0 \end{bmatrix}, \tag{25}$$

where the sign parameter $\sigma = \pm 1$ distinguishes between the focusing and defocusing equations. In terms of the spectral theory then, the distinction appears as a contrast between skew-Hermitian (focusing) and Hermitian (defocusing) scattering operators A_1.

As a solution method for pdes, the inverse spectral approach exploits a compatibility condition between two linear systems known as a Lax pair:

$$\vec{\psi}_x = \mathbf{L}\,\vec{\psi}; \qquad \vec{\psi}_t = \mathbf{B}\,\vec{\psi}. \tag{26}$$

The simultaneous eigenfunctions $\vec{\psi}(x,t)$ of these two linear operators are Jost, or in the periodic case, Bloch eigenfunctions. The temporal operator $\mathbf{B}$ is quadratic in the spectral parameter E:

$$\mathbf{B} = E^2 A_0 + E\, A_1 + A_2, \tag{27}$$

where

$$A_2 = -\frac{i}{4}\begin{pmatrix} -\sigma(|p|^2 + |q|^2) & -2p_x & -2q_x \\ -2\sigma p_x^* & \sigma|p|^2 & \sigma q p^* \\ -2\sigma q_x^* & \sigma q^* p & \sigma|q|^2 \end{pmatrix}. \tag{28}$$

The compatibility of the mixed partial derivatives in x and t requires that the potentials p and q in the scattering matrix A_1 must satisfy the coupled NLS system (2).

Periodic Spectral Theory

Fundamental to the inverse spectral theory is the mapping of the spatial structure of the complex potentials in $A_1(x,t)$ into spectral data via a Lax spectral problem. For

the coupled NLS with periodic boundary conditions, the third-order Lax problem is the linear ODE system (23) whose coefficients are periodic. Thus the natural tool for investigating the spectral properties is Floquet theory.

Consider the Lax spectral problem for fixed t,

$$\vec{\psi}_x = \mathbf{L}\vec{\psi}, \tag{29}$$

$$\vec{\psi}(x = x_o) = \vec{\psi}_o, \tag{30}$$

with solution

$$\vec{\psi} = \mathbf{M}(x; x_o)\vec{\psi}_o, \tag{31}$$

where the fundamental matrix solution is normalized by initial conditions to be the identity at $x = x_o$:

$$\mathbf{M}_x = \mathbf{L}\mathbf{M}, \tag{32}$$

$$\mathbf{M}(x = x_o) = \mathbf{I}. \tag{33}$$

For potentials $A_1(x)$ with period ℓ, the *Floquet multipliers* are simply the eigenvalues of the fundamental matrix solution taken over a single period as given by the characteristic polynomial

$$\det\left(\mathbf{M}(x_o + \ell; x_o) - \rho\mathbf{I}\right) = 0. \tag{34}$$

Alternatively, if the Floquet multipliers are distinct, solutions can be represented as a linear combination of the three independent *Floquet solutions*, each of which takes the form

$$\vec{\psi}(x) = e^{i\mu x}\hat{\psi}(x), \tag{35}$$

where the *Floquet exponents* μ are related to the multipliers by

$$\rho = e^{i\mu\ell}, \tag{36}$$

and $\hat{\psi}(x)$ has the same basic period ℓ.

Since the eigenvalue E appears within the Lax operator, the dependence of the Floquet solutions on this spectral parameter defines the *Floquet spectrum* — values of E at which a Floquet solution is bounded, or equivalently, $\mu(E)$ is real.

The Floquet spectrum is part of the Floquet multiplier curve: the Riemann surface constructed from the function elements $\rho(E)$, i.e. a three-sheeted covering of the complex sphere parametrized by the spectral parameter E. The Floquet spectrum consists of those values of E for which the modulus of the multiplier is unity; however, it is the Floquet multiplier curve as a whole, not merely the spectrum, that we use as our spectral information.

Three distinguished spectral elements are identified:

- *periodic/antiperiodic points* — values of E such that there is a periodic or anti-periodic eigenfunction, this corresponds to at least one $\mu(E)$ being an even/odd multiple of π/ℓ. The corresponding Floquet solutions will have the same/twice period of the complex potentials.

- *branch points* — values of E where two Floquet exponents μ are real and equal. These correspond to the endpoints of spectral branches; as well, each pair of branch points is associated with a Hamiltonian degree-of-freedom of the underlying coupled NLS wave.
- *Floquet double points* — values of E where the difference between two Floquet exponents $\triangle\mu$ is a multiple of $2\pi/\ell$, so that the multipliers ρ are degenerate. This spectrum is of importance in what follows; in particular, they represent locations where new branch points can be formed under perturbation. Thus they are critical to identifying which solutions can saturate the linear instabilities observed in the preceding sections for the plane wave. In fact, in the plane wave case, we show that there is a one-to-one correspondence between these double points and the Fourier modes of the eigenmode basis (for $\kappa \geq 0$ and for $\kappa \leq 0$ separately) and that *unstable modes are only associated with nonreal double points.*

A crucial difference between the Floquet spectrum of the scalar NLS and the coupled NLS is that for the scalar NLS the periodic/antiperiodic points are identical to the Floquet double points which contain the geometric information about the instability. This identity is due to the fact that in the 2×2 matrix case there is one linear constraint, viz. the sum of the μ is a multiple of $\frac{2\pi}{\ell}$, which is enough to fix the second μ if the first one is known to be a multiple of π/ℓ. In the 3×3 case there are three μ but still only one constraint, so that a periodic/antiperiodic point is no longer a location where the difference of a pair of μ is a multiple of $\frac{2\pi}{\ell}$.

Plane Wave Example

By way of illustation, the Floquet theory for the simple plane wave solution with equal amplitudes but equal and opposite wavenumbers (3) is presented:

$$p_o = a\, e^{i(+kx-\omega t)}; \qquad q_o = a\, e^{i(-kx-\omega t)}. \tag{37}$$

Although the Lax spectral problem is in general a nonconstant coefficient ODE, in the plane wave case, considerable simplification occurs in the explicit removal of the x-dependence via the transformation

$$\vec{\psi} = \begin{bmatrix} 1 & 0 & 0 \\ 0 & p_o^* & 0 \\ 0 & 0 & q_o^* \end{bmatrix} e^{i\mu x} \tilde{\psi},$$

where both the plane wave variations and Floquet exponential behaviors are incorporated. The vector $\tilde{\psi}$ is independent of x and is the eigenvector for the constant matrix problem

$$\begin{bmatrix} i\mu + \frac{2i}{3}E & -\frac{1}{2}a^2 & -\frac{1}{2}a^2 \\ \frac{\sigma}{2} & i\mu - i\,k - \frac{i}{3}E & 0 \\ \frac{\sigma}{2} & 0 & i\mu + i\,k - \frac{i}{3}E \end{bmatrix} \tilde{\psi} = \vec{0}. \tag{38}$$

The Floquet spectrum $\mu(E)$ is defined through the cubic characteristic polynomial

$$\mu^3 + \left(-\frac{1}{3}E^2 - k^2 - \frac{\sigma}{2}a^2\right)\mu + \frac{2}{27}E^3 - \frac{2}{3}Ek^2 + \frac{\sigma}{6}a^2 E = 0, \tag{39}$$

whereby, if the roots are distinct, the corresponding eigenvectors can be expressed in terms of the eigenvalue μ

$$\tilde{\psi} = \begin{pmatrix} -2i \\ \frac{\sigma}{\mu - k - \frac{1}{3}E} \\ \frac{\sigma}{\mu + k - \frac{1}{3}E} \end{pmatrix}. \tag{40}$$

By assembling a 3×3 diagonal matrix of Floquet multipliers ($\rho = e^{i\mu x}$) and a change of basis matrix whose columns are given by the corresponding eigenvectors,

$$\Lambda_\mu = \text{diag}(e^{i\mu x}), \tag{41}$$

$$\mathbf{S} = [\tilde{\psi}(\mu)], \tag{42}$$

the general solution for $\vec{\psi}$ can then be written in terms of a matrix of Floquet solutions and has the representation

$$\vec{\psi} = \begin{bmatrix} 1 & 0 & 0 \\ 0 & p_o^* & 0 \\ 0 & 0 & q_o^* \end{bmatrix} \mathbf{S} \Lambda_\mu \vec{c}, \tag{43}$$

where $\vec{c}$ is an arbitrary vector that provides a linear superposition of the Floquet eigenfunctions.

We can see clearly in this plane wave example that the Floquet multiplier $\rho(E)$ is determined by the spectral parameter E via the characteristic polynomial (39) for $\mu(E)$, the Floquet exponent, and the relation $\rho = e^{i\mu x}$. Thus for every E there are, in general, three function elements $\rho(E)$ which together form a three-sheeted covering of the complex sphere, i.e. the Floquet multiplier curve. The structure of this curve is given by a detailed analysis of the characteristic polynomial (39) for $\mu(E)$ so as to determine the following distinguished points:

- *Branch points* — points where $\mu(E)$ has a double root, so there is a square root type of singularity in the covering. There are exactly four such points, viz. the roots of the discriminant of the characteristic polynomial (39):

$$E^2 = \frac{-a^4 - 40\sigma a^2 k^2 + 32k^4 \pm a(\sqrt{a^2 - \sigma 16k^2})^3}{32k^2}. \tag{44}$$

- *Floquet double points* — points where two values of $\rho(E)$ are the same but the function elements are different. Under perturbations these points can split into pairs of branch points and hence they are important in identifying perturbations of the plane wave. Such points occur when two values of $\mu(E)$ differ by $\Delta = \frac{2\pi n}{\ell}$, n is an integer, for the same value of E. These double points occur when

$$E^2 = \frac{\left\{ a^4 - \sigma 12 a^2 \Delta^2 + 8\Delta^4 + \sigma 40 a^2 k^2 - 24\Delta^2 k^2 - 32k^4 \right.}{\left. \pm (a^2 + 4\sigma\Delta^2 - 16\sigma k^2)\sqrt{a^4 - 16\sigma a^2 k^2 + 16\Delta^2 k^2} \right\}} \\ -32k^2 + 8\Delta^2. \tag{45}$$

We are not concerned with antiperiodic/periodic points since, in the third order operator case, these do not correspond with the Floquet double points, as they do in the scalar NLS case with a second order spectral operator. What we are interested in is locations where new branch points can develop under perturbations, viz. the double points. Heuristically, a splitting of a double point where two values of $\mu(E)$ differ by $\Delta = \frac{2\pi n}{\ell}$ should correspond to a perturbation by an eigenmode proportional to $\delta\rho = e^{i\Delta x}$. Indeed, although we do not pursue the details here, there is an explicit mapping by which each linearized CNLS system eigenmode is constructed from products of the Floquet eigenvectors, evaluated at a corresponding Floquet double point.

Remark. It is immediately obvious from equations (44) and (45) that the branch points are the endpoints of the sequence of Floquet double points occurring when $\Delta^2 = 0$. If Δ^2 is considered as a continuous real parameter that denotes the (squared) difference between two values of μ on the three-sheeted covering at the same E value, then we can imagine the double points as a continuous stream flowing out of the branch points and circulating throughout the three sheets of the branched covering. Near branch points, the double points will necessarily connect the same two sheets of the curve as their parent branch point. However at turning points where $\frac{dE}{d(\Delta^2)} = 0$ and $\frac{dE}{d(\Delta^2)}$ changes sign, there will be a sheet change, i.e. the pair of sheets whose separation is given by Δ^2 will necessarily change at such points (two distinct values of Δ^2 on either side of the turning point must represent the difference of μ values between two distinct pairs of sheets over the same value of E). In this way we can identify which sheets the double points are connecting as they flow throughout the curve.

1-1 Correspondence of Eigenmodes and Double Points

Note that for every eigenmode frequency $\kappa \geq 0$ (and similarly for $\kappa \leq 0$) there are precisely four eigenmodes in the complete eigenmode basis given by equation (20) in terms of the four distinct roots of the dispersion relation (11).

For clarity we assume that the four roots of the dispersion relation (11) are distinct, although the extension to degenerate roots is straightforward. If we now set $\Delta^2 = \kappa^2 > 0$ in equation (45) for the locations of the double points, we obtain precisely four double points corresponding to the four eigenmodes. At this point the solutions of the linearized CNLS system could be constructed from products of the eigenvectors of the Lax pair evaluated at the corresponding spectral double points. However for the purposes of constructing the *nonlocal* behavior of the instabilities via Bäcklund transformations, it is sufficient to note that under this correspondence, for perturbed plane waves, *there are unstable eigenmodes if and only if there are nonreal double points*.

The only exception to this simple state of affairs occurs when $\Delta^2 = \kappa^2 = 0$, in which case the double points become branch points and the system is modulationally unstable (i.e. possesses a long-wave instability) *if and only if* at least two of the branch points are complex, as was shown by one of us in [40].

- In particular, the defocusing case ($\sigma = -1$) has a band of nonreal double points corresponding to unstable eigenmodes precisely when $4k^2 - 2a^2 < \Delta^2 < 4k^2$ in agreement with the relation (17) describing the cross-phase resonance.

- Note that if $0 < 4k^2 - 2a^2$ then this instability is at *intermediate* wavenumbers, and the sideband of unstable eigenmodes that appears in the defocusing instability diagram, Figure 1, does not not extend to the $\kappa = 0$ wavenumber. Thus this instability is *not* the traditional long-wave modulational instability that appears in the focusing equations. In particular, all the branch points are real in this case and a modulational stability analysis of long waves would predict modulational stability, even though there are intermediate wavelength perturbations to which the system is unstable.
- In the section on *Commutator Spectral Theory* we show how the integrable nature of the CNLS system can be used to generate equations with quasi-periodic solutions which saturate the cross-phase instability of this plane wave example.

Homoclinic Orbits and Bäcklund Transformations

Now that the spectral elements in the integrable theory that correspond to linearized instabilities have been identified, a Bäcklund transformation can be used to generate the nonlocal dynamics for the simplest unstable configurations. In particular, for plane waves of equal amplitude, restricted to a small spatially periodic domain $0 < x < 2\pi$, most of the long-wavelength instabilities will be *cut off* and only a few modes will evolve to nonlinear amplitudes — this should lead to dynamics with the minimum amount of complexity. This is an especially likely situation in integrable systems, where the existence of the infinite hierarchy of conservation laws places a greater restriction on the allowable dynamics.

Defocusing Case

The defocusing system has only one kind of instability present, as shown in Figure 1: a cross-phase instability of dimension one for each unstable wavenumber. (Note that because of the symmetry of the system, eigenmodes come in pairs corresponding to $\pm\kappa$.) To examine the nonlocal nature of instability, three cases are considered for a fundamental mode with equal intensity in the two channels,

$$p = ae^{i(kx-\omega t)}, \qquad q = ae^{i(-kx-\omega t)}.$$

- In the instability diagram Figure 1, let the wave parameters be $\frac{k}{|a|} = \frac{\kappa}{|a|} = \frac{1}{\sqrt{2}}$, $k = \kappa = 1$, with period $L = 2\pi$. In this case, all four branch points are real, but two of them double up at the origin, so this wave is marginally unstable to zero wavenumber disturbances. Locating the discrete set of eigenmode wavenumbers for these parameters on Figure 1 shows that there are exactly two unstable eigenmodes, one for each of the first harmonics $\kappa = \pm 1$, and these correspond to precisely one complex pair of Floquet double points on the imaginary axis. The second harmonic is marginally stable (two double points meet at the point over infinity on the Riemann sphere), and all the higher harmonics are neutrally stable (the corresponding double points are on the real axis.) Using an imaginary Floquet double point of the single complex conjugate pair present in the spectrum in a Bäcklund transformation [12], [35] of the original plane wave, a homoclinic orbit is generated that approaches the

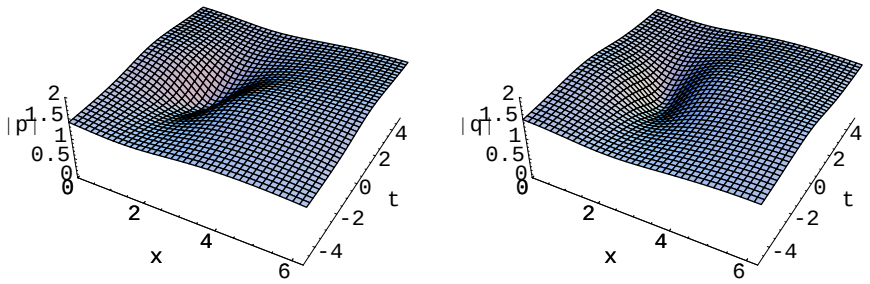

Fig. 6. Defocusing Homoclinic Orbit of an unstable first harmonic eigenmode at $\frac{k}{|a|} = \frac{\kappa}{|a|} = \frac{1}{\sqrt{2}}$ in the instability diagram (Fig. 1). Notice that the two channels are equally excited by the instability, indicating the essential cross-phase nature of the instability. The homoclinic orbit can be spatially translated because of the presence of an arbitrary phase shift in the perturbation. Using the second member of the Floquet double point conjugate pair in the Bäcklund transformation results in a phase shift; see Figure 7.

plane wave as time goes to positive and negative infinity; see Figure 6. If the conjugate double point of the pair is used in the Bäcklund transformation, then the same orbit is obtained, only spatially translated (see Fig. 7), corresponding to the fact that there is an asymptotically stable eigenmode (thus unstable in negative time) which produces a spatial perturbation in $|p|$ and $|q|$ that is merely a phase shift of the previous unstable eigenmode.

- Two other cases are considered of an unstable first harmonic in the defocusing case, illustrating the deformation of the homoclinic orbits as the wavenumbers are varied. Figure 8 shows the evolution of smaller scales at $\frac{k}{|a|} = \frac{\kappa}{|a|} = .4$, with $k = \kappa = 1$ and $|a| = \frac{10}{4}$ on a period of $L = 2\pi$; the smaller scales are indicative of the broadening of the unstable band of wavenumbers.
- Figure 9 shows the evolution of longer scales at $\frac{k}{|a|} = \frac{\kappa}{|a|} = .8$, with $k = \kappa = 1$ and $|a| = \frac{10}{8}$ on a period of $L = 2\pi$; the longer scales are indicative of the decrease in the width of the unstable band of wavenumbers.

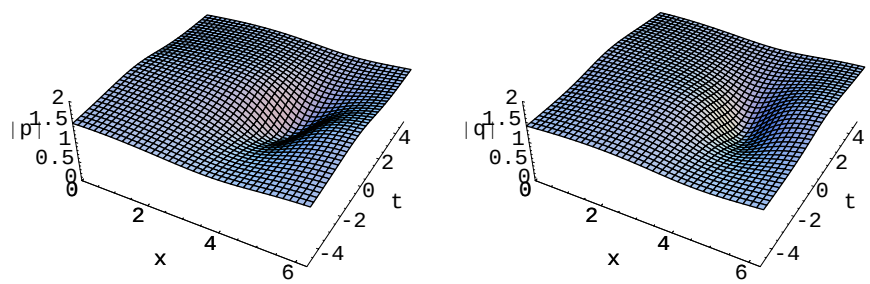

Fig. 7. Defocusing Homoclinic Orbit with phase shift, corresponding to the same instability appearing in Figure 6.

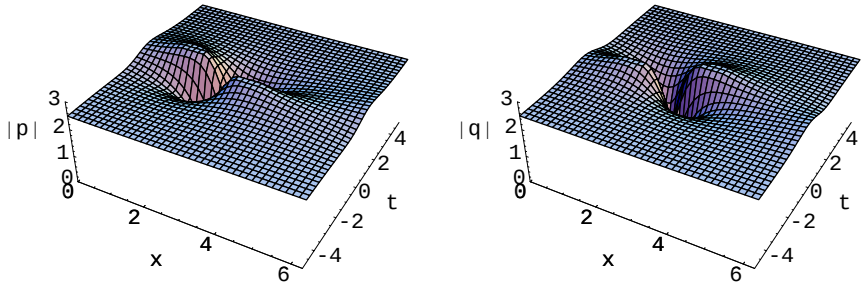

Fig. 8. Defocusing Homoclinic Orbit of an unstable first harmonic eigenmode at $\frac{k}{|a|} = \frac{\kappa}{|a|} = .4$ in the instability diagram. Notice the increase in fine-scale structure.

All the solutions generated by the Bäcklund transformation illustrate that each unstable manifold of the plane wave contains a homoclinic orbit: The solutions asymptote back to the plane wave along the direction of a stable eigenmode.

Moreover, the disturbance has the same maximum magnitude in the two channels, indicative of the cross-phase mechanism of the instability in which both channels are equally excited.

The orbits in a finite-dimensional function space neighbourhood of the first of the homoclinic orbits considered above, corresponding to orbits in the saddle of two crossed homoclinic orbits (as in the phase plane of the unforced Duffing equation), are generated later using the *stationary equations* of the integrable hierarchy.

Focusing Case with Equal Intensities in the Fundamental Mode

The focusing system with equal intensities in the fundamental mode,

$$p = ae^{i(kx-\omega t)}, \qquad q = ae^{i(-kx-\omega t)},$$

is considered for two different sets of wave parameters, in order to illustrate the different regions of instability described in Figure 3.

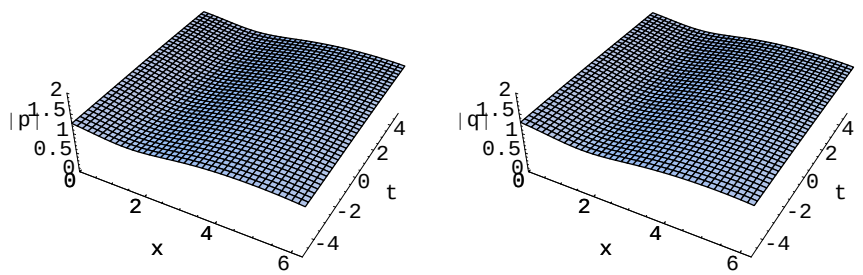

Fig. 9. Defocusing Homoclinic Orbit of an unstable first harmonic eigenmode at $\frac{k}{|a|} = \frac{\kappa}{|a|} = .8$ in the instability diagram. Notice the increase in large-scale structure.

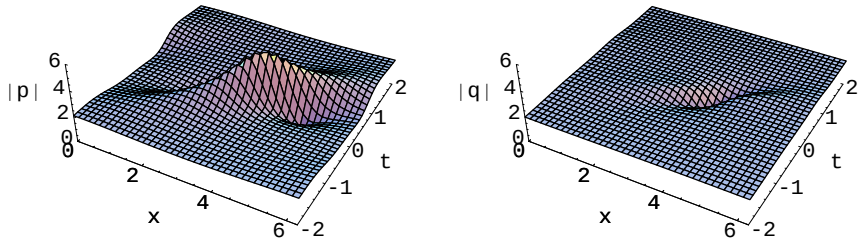

Fig. 10. Self-Phase Focusing Homoclinic Orbit I from an unstable first harmonic eigenmode ($k/|a| = .5$, $\kappa/|a| = \pm.5$) in the self-phase W_u^2 region of Figure 3. Notice that most of the oscillations are trapped in the p-channel. The Floquet double point corresponding to the unstable first harmonic eigenmode generating this homoclinic orbit is at $-.498 + 1.89i$ in Figure 16. Compare with Figure 11.

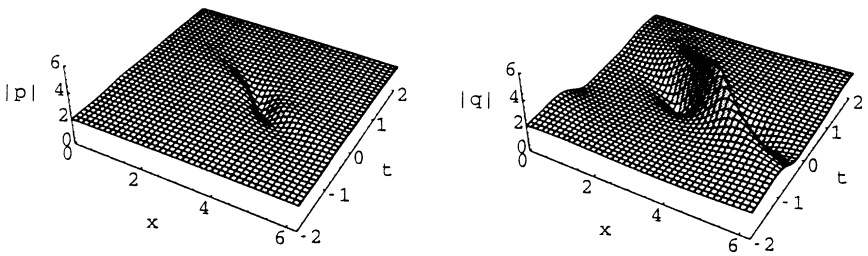

Fig. 11. Self-Phase Focusing Homoclinic Orbit II from the other unstable first harmonic eigenmode ($k/|a| = .5$, $\kappa/|a| = \pm.5$) in the self-phase W_u^2 region of Figure 3. Notice that the instability is mostly confined to the q-channel. The Floquet double point corresponding to the unstable first harmonic eigenmode saturated by this homoclinic orbit is at $.498 + 1.89i$ in Figure 16. Compare with Figure 10.

- The focusing system with $a = 2$ and $k = 1$ and period $L = 2\pi$ is considered. The first harmonic ($\frac{k}{|a|} = \frac{\kappa}{|a|} = \frac{1}{2}$) lies in self-phase W_u^2 region of Figure 3 and generates two unstable eigenmodes due to the classical self-phase Benjamin-Feir long-wave instability. *Individual perturbations of this type can produce very little energy transfer between the two channels, indicating the self-phase nature of the instability.* Of course a composition of the two different instabilities in the pair could be chosen to reveal the coupling of the equations. See Figure 10, in which the effects of the modulational instability are mostly confined to the p channel of the coupled system. In Figure 11 the oscillations arising from the instability are primarily restricted to the q channel.

  The second harmonic is, as always when the amplitudes of the two channels are equal, marginally stable.

  The third harmonic $\frac{k}{|a|} = \frac{1}{2}$ and $\frac{\kappa}{|a|} = \frac{3}{2}$ lies in cross-phase W_u^1 sideband of Figure3 and has exactly one unstable eigenmode due to the cross-phase resonance. *Energy is necessarily transferred between the two channels, indicating the essential cross-phase nature of the instability.* See Figure 12.

  The fourth and higher harmonics are all stable.

  The low harmonics correspond to Floquet spectral data as shown in Figure 16.

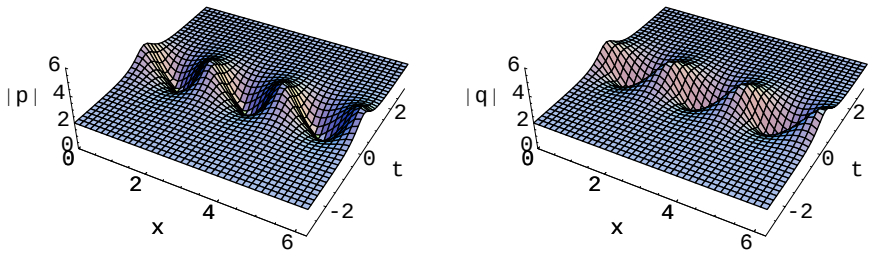

Fig. 12. Cross-Phase Focusing Homoclinic Orbit of the unstable third harmonic ($k/|a| = .5$ and $\kappa/|a| = \pm 1.5$) in the cross-phase W_u^1 sideband of Figure 3. Notice that energy is necessarily transferred between the two channels, indicating the cross-phase nature of the instability excited by this harmonic. The Floquet double point corresponding to the unstable third harmonic eigenmode saturated by this homoclinic orbit is at $1.51i$ in Figure 16.

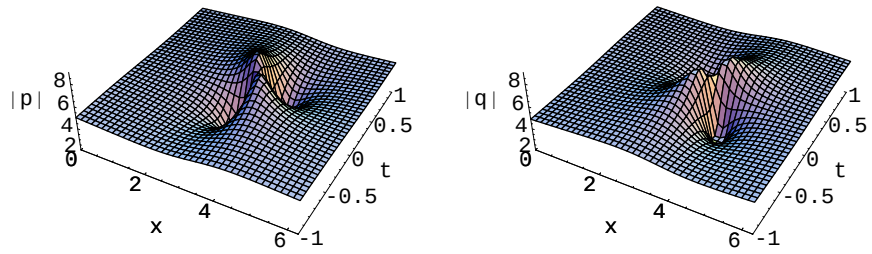

Fig. 13. Cross-Phase Focusing Homoclinic Orbit (large-scale disturbance) of an unstable first harmonic ($k/|a| = .2$ and $\kappa/|a| = \pm .2$) from the cross-phase W_u^2 region of Figure 3; see also Figure 14 for the second unstable mode that produces a smaller scale disturbance.

- The focusing system with $a = 5$ and $k = 1$ and period $L = 2\pi$ is considered. In this case the first harmonic $\frac{k}{|a|} = \frac{\kappa}{|a|} = .2$ is in the cross-phase W_u^2 region of Figure 3. There are two unstable cross-phase modes. Both modes equally excite the two channels but one mode (Fig. 13) produces a larger, broader disturbance than the other mode (Fig. 14). The third harmonic $\frac{\kappa}{|a|} = .6$ lies in the cross-phase W_u^1 region and has one unstable cross-phase mode that equally excites the two channels (Fig. 15).

Focusing Case with Unequal Intensities in the Fundamental Mode

The focusing case is considered for two different fundamental modes with unequal intensity division,

$$p = ae^{i(kx-\omega t)}, \qquad q = be^{i(-kx-\omega t)},$$

for which $|a|^2 = 10|b|^2$, in order to illustrate the regions of instability in Figure 4.

- In order to select modes in a vertical slice of the instability diagram where $\frac{k}{|a|} = .6$, with modes in the self-phase W_u^2 region, the self-phase W_u^1 region, and the cross-phase W_u^1 sideband, we choose $|a| = \frac{5}{3}$, $|b| = \frac{5}{3\sqrt{10}}$, $L = 6\pi$, and $k = 1$. Thus, in Figure 4, this case corresponds to $\frac{k}{|a|} = .6$ and the n-th harmonic is $\frac{\kappa}{|a|} = .2n$. The first harmonic

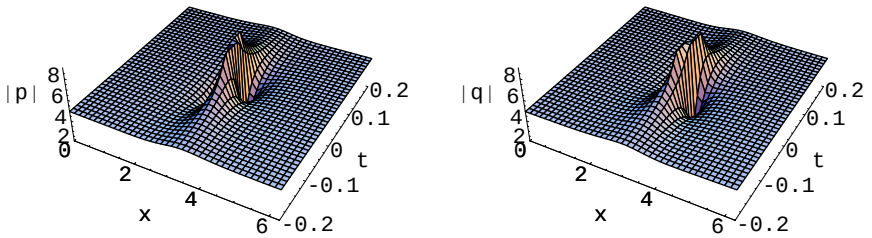

Fig. 14. Cross-Phase Focusing Homoclinic Orbit (small scale disturbance) of an unstable first harmonic ($k/|a| = .2$ and $\kappa/|a| = \pm.2$) from the cross-phase W_u^2 region of Figure 3; see also Figure 13 for the other unstable first harmonic eigenmode.

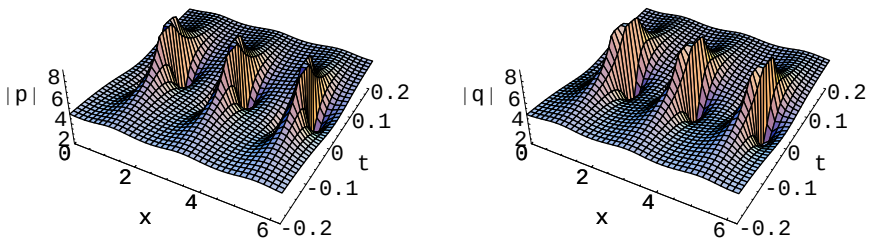

Fig. 15. Cross-Phase Focusing Homoclinic Orbit of the unstable third harmonic ($k/|a| = .2$ and $\kappa/|a| = \pm.6$) from the cross-phase W_u^1 region of Figure 3.

is in the narrow doubly unstable self-phase W_u^2 band near the $k/|a|$ axis and has two independent unstable modes; the resulting homoclinic orbits are shown in Figures 17 and 18. The second, third, and fourth harmonics are all in the wider unstable self-phase W_u^1 band that remains in the scalar limit when $|b| \to 0$ and each harmonic generates one instability. The third harmonic instability is shown in Figure 19. The fifth harmonic is neutrally stable and the sixth harmonic is marginally stable. The seventh harmonic lies in the narrow cross-phase W_u^1 instability sideband that disappears in the scalar limit, and it has one instability associated with it, as shown in Figure 20.

All higher harmonics are neutrally stable.

- To select modes in a vertical slice of the instability diagram passing through the transition or mixed regions, we choose $a = \frac{10}{3}$ and $b = \frac{\sqrt{10}}{3}$, $L = 6\pi$, and $k = 1$. Thus, in Figure 4, this case corresponds to $\frac{k}{|a|} = .3$ and the n-th harmonic is $\frac{\kappa}{|a|} = .1n$. The first harmonic has a two-dimensional instability in the mixed W_u^2 central region; see Figures 21 and 22. Both the third harmonic (Fig. 23) and the seventh harmonic (Fig. 24) are in the transition W_u^1 region between the cross-phase sideband and the self-phase central band of W_u^1, and each generates one unstable transitional type of cross-phase instability. Harmonics twelve and above are stable.

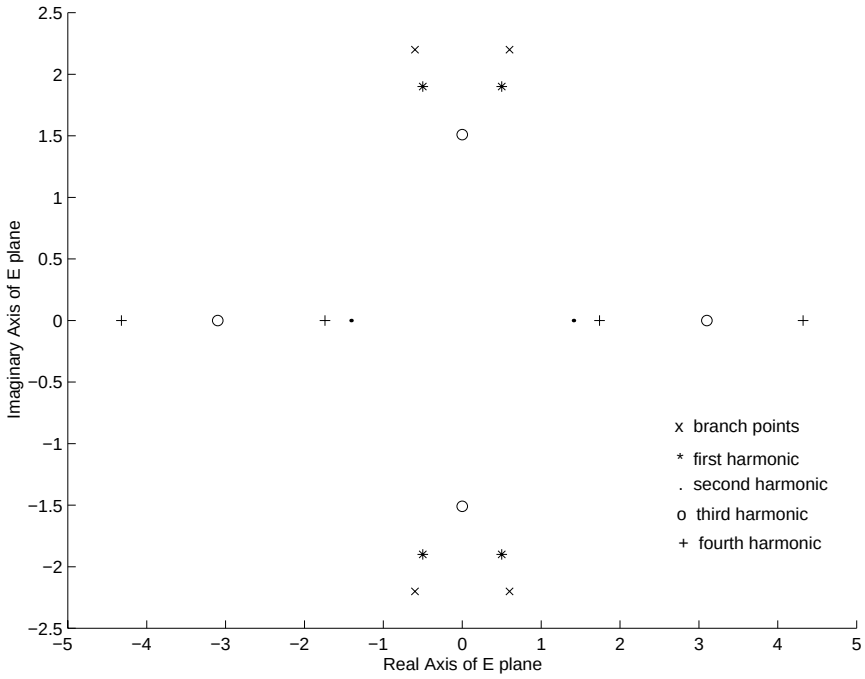

Fig. 16. The Floquet spectrum of the focusing plane wave with equal intensities ($a = b = 2$, $k = 1$, and $L = 2\pi$), labeled by the associated eigenmodes from the linearized equations. The branch points correspond to the spatially independent fundamental mode. The four modes of a harmonic with wavenumber κ correspond to quartets of double points in the spectrum (note that the modes of κ and $-\kappa$ correspond to the same quartet). A complex conjugate pair of double points indicates an unstable mode and one asymptotically stable mode. A real pair of double points indicates neutral stability. The first harmonic has two independent self-phase instabilities for each of $\kappa = \pm 1$, although the perturbations of $\kappa = -1$ are merely phase-shifted versions of those of $\kappa = +1$. The second harmonic has two double points on the real axis corresponding to neutrally stable modes, and a second pair of double points have coalesced along the real axis at $\pm\infty$ corresponding to marginally stable modes. This pair of double points reappears along the imaginary axis to produce the pure cross-phase instability of the third harmonic. The modes of the fourth and higher harmonics are all neutrally stable, and are associated with real double points.

Commutator Spectral Theory

The homoclinic orbits to the plane wave solutions of the CNLS system that were constructed using Bäcklund transformations indicate the presence of crossed homoclinic saddles in the phase space of the coupled system. The structure of these saddles is qualitatively similar to that of the critical point in the phase plane of the unforced Duffing oscillator. To generate the near-homoclinic orbits of the coupled system and clarify the saddle structure of part of the phase space, it is necessary to generate a class of quasi-periodic solutions known as N-phase waves and restrict them to the simplest spatially periodic subclass that contains the homoclinic orbit. Such quasi-periodic solutions obey *stationary equations* of the CNLS hierarchy of integrable flows. The correct stationary

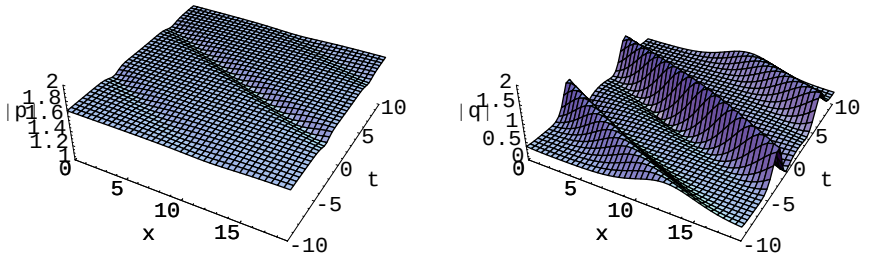

Fig. 17. Self-Phase Focusing Homoclinic Orbit, with unequal intensities in the plane waves of the two channels, for one of the first harmonic unstable modes in the self-phase W_u^2 region of Figure 4. Notice that most of the oscillations generated by the instability are trapped in the q-channel, even though the background plane wave in the q-channel is smaller in absolute magnitude than in the p-channel. Compare with Figure 18.

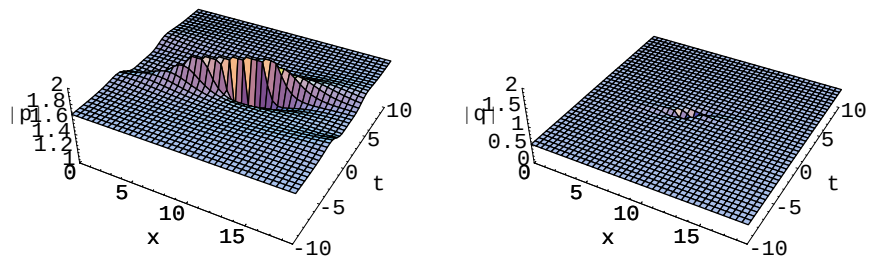

Fig. 18. Self-Phase Focusing Homoclinic Orbit, with unequal intensities in the plane waves of the two channels, for the other first harmonic unstable mode in the self-phase W_u^2 region of Figure 4. Notice that most of the oscillatory behavior is trapped in the p-channel. Compare with Figure 17.

equations can be identified via the spectral data of the unstable plane wave, in particular the location of the branch points and the double points of the associated unstable eigenmodes on the Floquet curve. The stationary equations also have an invariant curve, which for periodic potentials must have branch points matching those in the Floquet spectrum of the potentials.

In order to construct such quasi-periodic solutions, it is convenient to restate the Lax pair in matrix form, and hence construct the stationary equations. A fuller discussion of the stationary equations of the CNLS is contained in [41].

The CNLS system is equivalent to the compatibility of the following commutator Lax pair:

$$\mathbf{Q}_x = [\mathbf{L}, \mathbf{Q}] \qquad \text{and} \qquad \mathbf{Q}_t = [\mathbf{B}, \mathbf{Q}]. \tag{46}$$

Just as the special soliton solutions of the focusing NLS equation are associated with the reflectionless eigensolutions, *the fundamental solutions of the quasi-periodic NLS are generated through special matrices* $\mathbf{Q}$ *whose representations are polynomials in the scattering eigenvalue* E — these are more commonly referred to as *N-phase waves*. The 0-phase waves are simply the exponential plane waves.

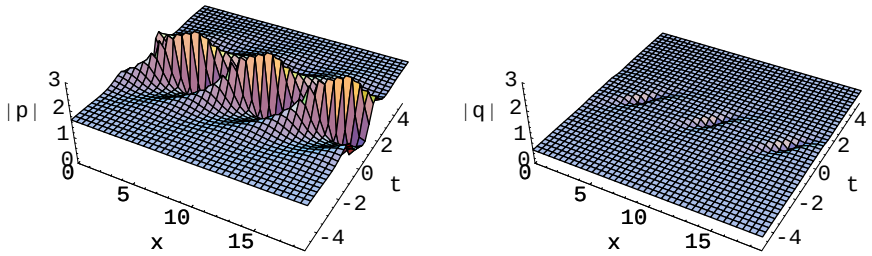

Fig. 19. Self-Phase Focusing Homoclinic Orbit, with unequal intensities in the plane waves of the two channels, for the third harmonic instability in the self-phase W_u^1 region of Figure 4. Notice that self-phase oscillations are trapped in the p-channel. Moreover, there is no mode which traps oscillatory behavior in the q-channel for this harmonic.

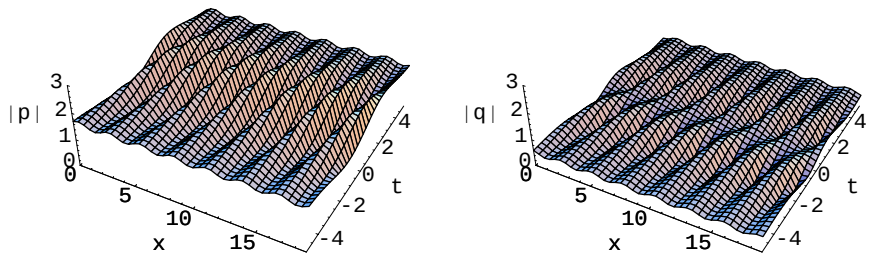

Fig. 20. Cross-Phase Focusing Homoclinic Orbit, with unequal intensities in the plane waves of the two channels, for the seventh harmonic instability in the cross-phase W_u^1 sideband of Figure 4. Notice that energy is equally shared between the two channels. This indicates the cross-phase nature of the instability in this harmonic.

Our present working hypothesis is that the N-phase waves for the coupled NLS equations provide the natural resolution for the breakdown of the nonlinear WKB analysis of the birefringent fiber system.

As we have seen, the defocusing CNLS system has a plane wave solution with double points corresponding to linear instabilities with frequencies in the band $4k^2-2a^2 < \kappa^2 < 4k^2$. These complex double points occur in conjugate pairs. We will present a simple class of N-phase waves which result from the perturbation that excites the unstable modes of the first harmonic of a plane wave solution of the defocusing CNLS system. The plane wave is chosen to have exactly two complex double points in its spectrum associated with exactly one unstable mode in the first harmonic, all other eigenmodes being stable, thus reducing the complexity of the dynamics. The choice of parameters is precisely the same as for the defocusing plane wave solution generated in Figures 6 and 7 in the section on *Bäcklund Transformations and Homoclinic Orbits*. This particular plane wave has four real branch points, two of which have come together over the origin of the E plane. This choice was not accidental, but was made for technical reasons, since the stationary equations that we construct have an additional degree of freedom corresponding to a double point at the origin, in addition to the required four branch points and the two complex double points of the instability. By placing the branch points at the same location as the unwanted double point, this extra degree of freedom produces

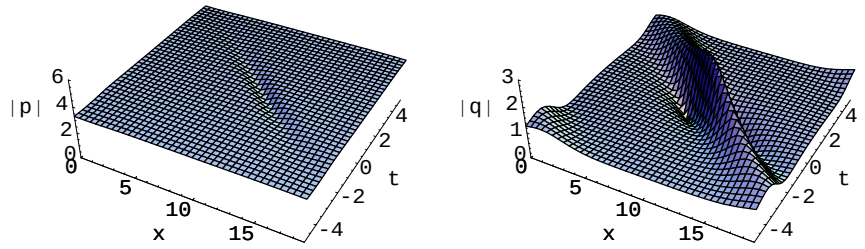

Fig. 21. Focusing Homoclinic Orbit, with unequal intensities in the plane waves of the two channels, for a first harmonic instability in the mixed W_u^2 region of Figure 4. Notice the self-phase behavior of the oscillations which occur predominately in the q-channel. Compare with Figure 22.

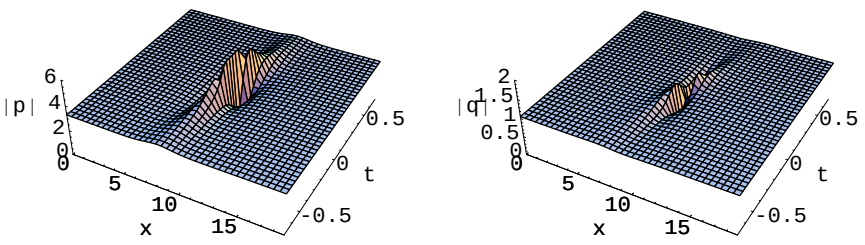

Fig. 22. Focusing Homoclinic Orbit, with unequal intensities in the plane waves of the two channels, for the other first harmonic instability in the mixed W_u^2 region of Figure 4. Notice the transitional nature of the relative energy transfer between the two channels: There is a cross-phase excitation of both channels, but the initially larger in magnitude p-channel tends to dominate. Also the oscillations are small in scale, similar to the third harmonic that lies in the transitional W_u^1 region of the cross-phase sideband (Fig. 23). Compare with Figure 21.

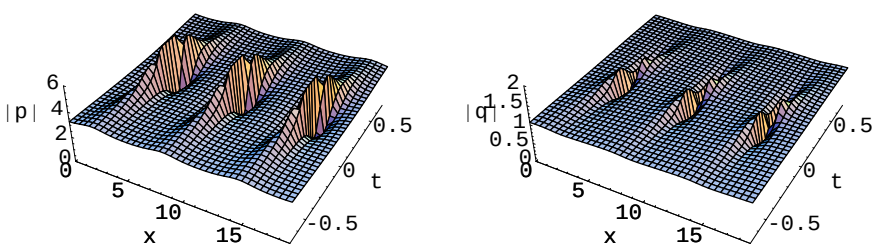

Fig. 23. Focusing Homoclinic Orbit, with unequal intensities in the plane waves of the two channels, for the third harmonic instability in the transitional W_u^1 region of the cross-phase sideband in Figure 4. Notice that energy is necessarily transferred between the two channels and that the oscillations are small in scale. This indicates the transitional cross-phase nature of the instability in this harmonic.

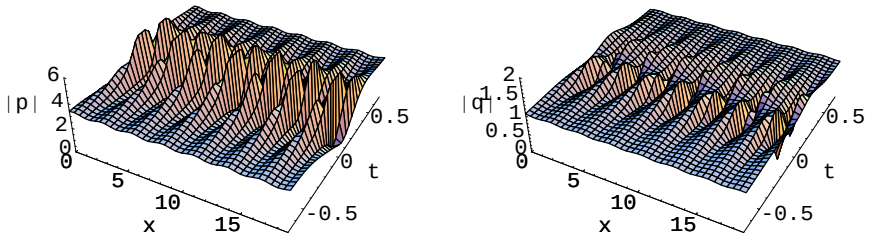

Fig. 24. Focusing Homoclinic Orbit, with unequal intensities in the plane waves of the two channels, for the seventh harmonic instability in the transitional W_u^1 region of the cross-phase sideband in Figure 4. Notice that energy is necessarily transferred between the two channels. This indicates the transitional cross-phase nature of the instability in this harmonic.

effects of smaller order than the instability excited by small perturbations, since the double points of the unstable mode and the branch points are separated by O(1).

It is an open problem to find stationary equations whose invariant curve is precisely equivalent to any given set of spectral data. The construction of angle-like variables that linearize the flow of an arbitrary set of stationary equations via the Abel-Jacobi map on the Jacobian of the invariant spectral curve (representing the action variables) has been carried out for a certain class of solutions by Adams et al. [3], [4].

N-Phase Waves

If we assume that $\mathbf{Q} = \mathbf{Q}^0 + \mathbf{Q}^1 E^{-1} + \mathbf{Q}^2 E^{-2} + \mathbf{Q}^3 E^{-3} + \cdots$, then the x-flow of equation (46) produces the following recursion relations for the entries q_{ij}^n of $\mathbf{Q}^n$:

$$
\begin{aligned}
&\text{(off-block entries)}\\
q_{12}^{n+1} &= i\partial q_{12}^n - \frac{i}{2}p(q_{22}^n - q_{11}^n) - \frac{i}{2}qq_{32}^n,\\
q_{13}^{n+1} &= i\partial q_{13}^n - \frac{i}{2}q(q_{33}^n - q_{11}^n) - \frac{i}{2}pq_{23}^n,\\
q_{21}^{n+1} &= -i\partial q_{21}^n - \frac{i}{2}r(q_{22}^n - q_{11}^n) - \frac{i}{2}sq_{23}^n,\\
q_{31}^{n+1} &= -i\partial q_{31}^n - \frac{i}{2}s(q_{33}^n - q_{11}^n) - \frac{i}{2}rq_{32}^n,\\
&\text{(block entries)}\\
q_{11}^{n+1} &= -q_{22}^{n+1} - q_{33}^{n+1},\\
q_{22}^{n+1} &= \frac{1}{2}\partial^{-1}(-pq_{21}^{n+1} + rq_{12}^{n+1}) + i\alpha,\\
q_{33}^{n+1} &= \frac{1}{2}\partial^{-1}(-qq_{31}^{n+1} + sq_{13}^{n+1}) + i\delta,
\end{aligned}
$$

$$q_{23}^{n+1} = \frac{1}{2}\partial^{-1}(-qq_{21}^{n+1} + rq_{13}^{n+1}) + i\beta,$$
$$q_{32}^{n+1} = \frac{1}{2}\partial^{-1}(-pq_{31}^{n+1} + sq_{12}^{n+1}) + i\gamma,$$

where $r = -\sigma p^*$ and $s = -\sigma q^*$, and α, β, γ, and δ are constants of integration.

If $\mathbf{Q}$ is truncated and forced to be a finite Laurent expansion in E, then this forces the potentials p and q to satisfy additional constraints that define the multiphase wave. These additional constraints are called the *stationary equations* and are, in general, integro-differential equations. For a systematic development of the construction of stationary equations for the CNLS system, see Wright [41]. The crucial point is that the characteristic polynomial of $\mathbf{Q}$ has the same *branch points* as the Floquet multiplier curve of the periodic potentials, so we can identify the N-phase wave resulting from a given perturbation by checking the location of its branch points in the limit where the solution degenerates to the plane wave. A simple N-phase wave that has the correct branch point structure, modulo the technical difficulty of an extra double point at the origin, to match the perturbation of the defocusing plane wave with exactly one unstable harmonic, is given by a quadratic ansatz in E^{-1}:

$$\mathbf{Q} = \mathbf{Q}^0 + \mathbf{Q}^1 E^{-1} + \mathbf{Q}^2 E^{-2}.$$

When $\mathbf{Q}$ is given by the above ansatz, certain integro-differential constraints must be satisfied by the solution of the CNLS system. These constraints define the N-phase wave, given that the perturbed plane wave must also satisfy the constraints to first order in the perturbation. The constraints can be given as

$$\begin{aligned} 0 &= -2p_{xx} + 4i(1+\alpha)p_x + 6\alpha p + p(|p|^2 + |q|^2) \\ &\quad - 2i(1+\alpha)q\int^x pq^* dx, \qquad (47) \\ 0 &= -2q_{xx} - 4i(1+\alpha)q_x + 6\alpha q + q(|p|^2 + |q|^2) + 2i(1+\alpha)p\int^x qp^* dx, \end{aligned}$$

in which the parameter $\alpha = \frac{1}{4}(1 - \sqrt{13})$. Of course the t-flow constraints (which we do not write out explicitly) are compatible with the x-flow constraints if and only if the solution is a solution of the CNLS system.

Finally, given the linear perturbation $p = p_0(1 + \tilde{p})$ and $q = q_0(1 + \tilde{q})$ where

$$\tilde{p} = f_+ e^{i\kappa x} + f_-^* e^{-i\kappa x},$$
$$\tilde{q} = g_+ e^{i\kappa x} + g_-^* e^{-i\kappa x},$$

there are two independent unstable perturbations v_1 and v_2 with $\kappa = 1$. One mode is a pure growth mode in positive time with $\Omega = i\sqrt{-7 + 2\sqrt{13}}$ and the second is a pure decay mode in positive time with $\Omega = -i\sqrt{-7 + 2\sqrt{13}}$.

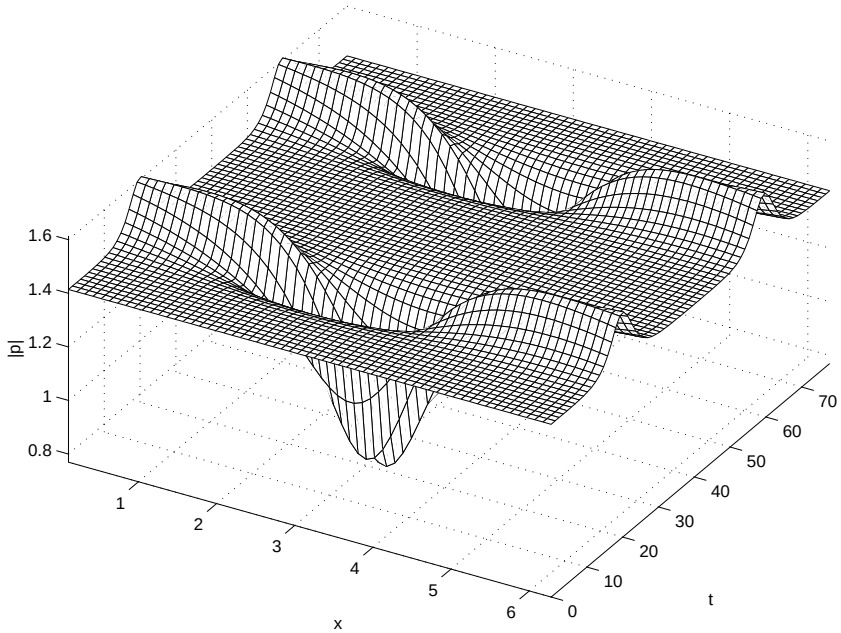

Fig. 25. Evolutionary dynamics in the nonlocal manifold near the plane wave instability — *inside* the homoclinic orbit (p-channel).

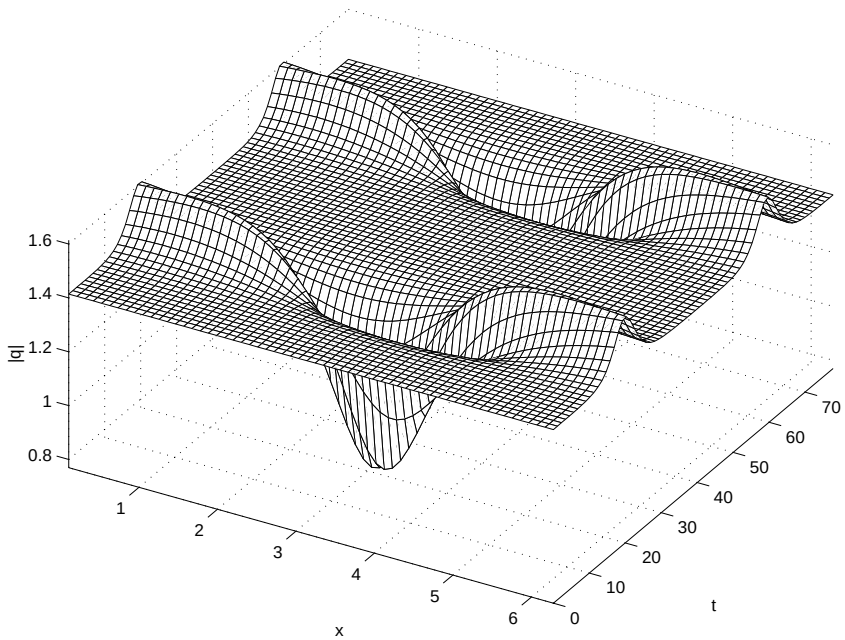

Fig. 26. Evolutionary dynamics in the nonlocal manifold near the plane wave instability — *inside* the homoclinic orbit (q-channel).

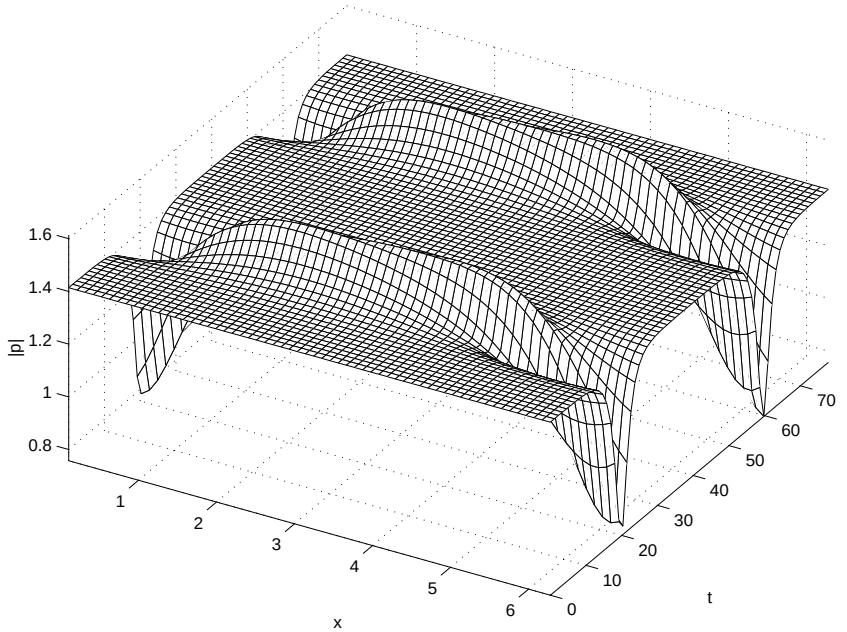

Fig. 27. Evolutionary dynamics in the nonlocal manifold near the plane wave instability — *inside* the homoclinic orbit (p-channel).

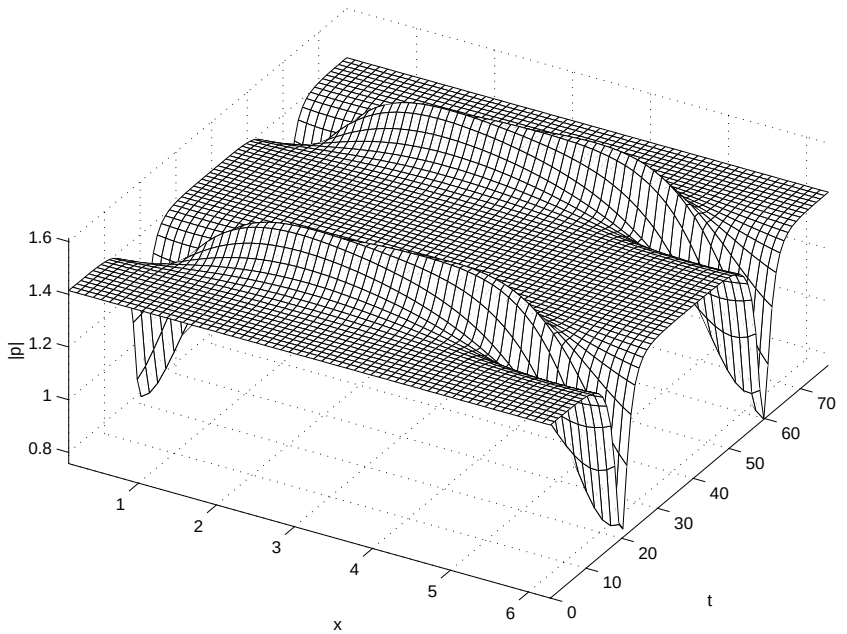

Fig. 28. Evolutionary dynamics in the nonlocal manifold near the plane wave instability — *inside* the homoclinic orbit (q-channel).

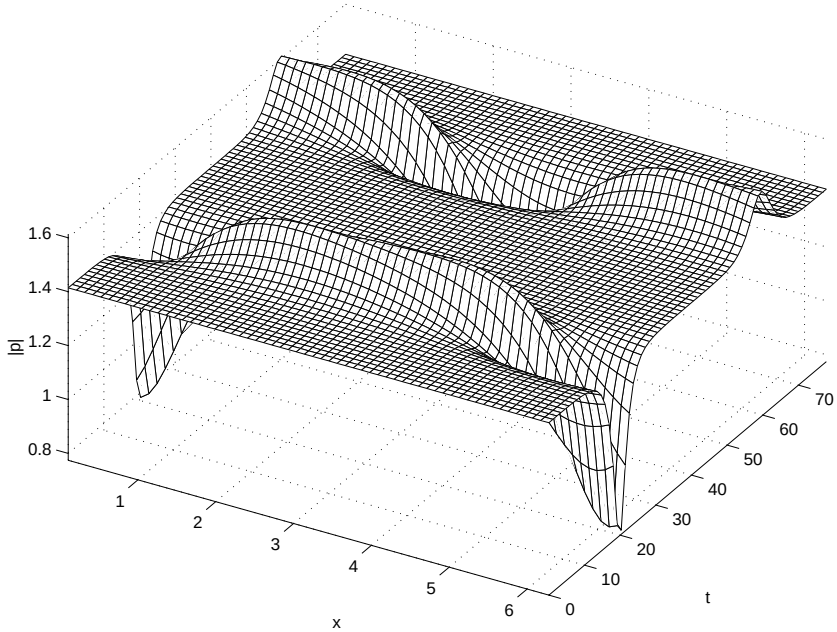

Fig. 29. Evolutionary dynamics in the nonlocal manifold near the plane wave instability — *outside* the homoclinic orbit (p-channel).

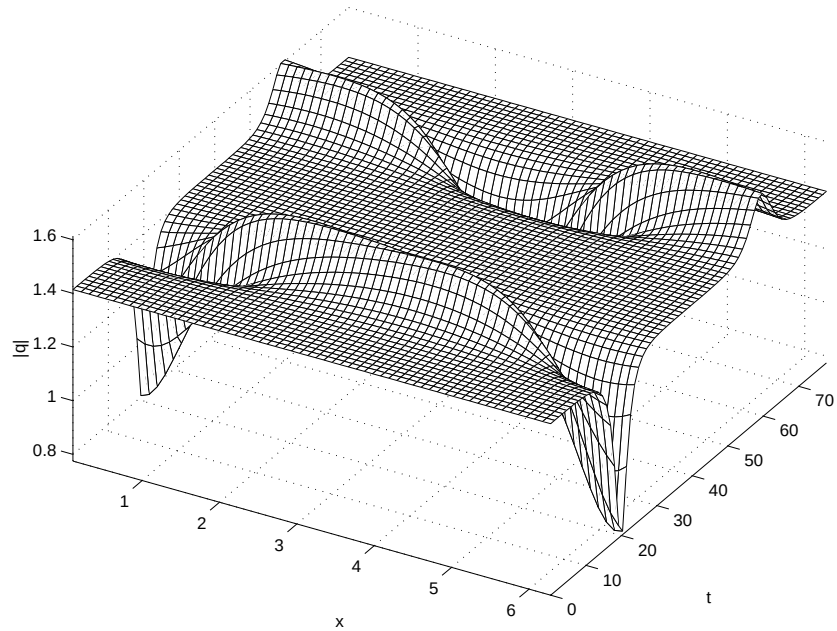

Fig. 30. Evolutionary dynamics in the linearized manifold near the plane wave instability — *outside* the homoclinic orbit (q-channel).

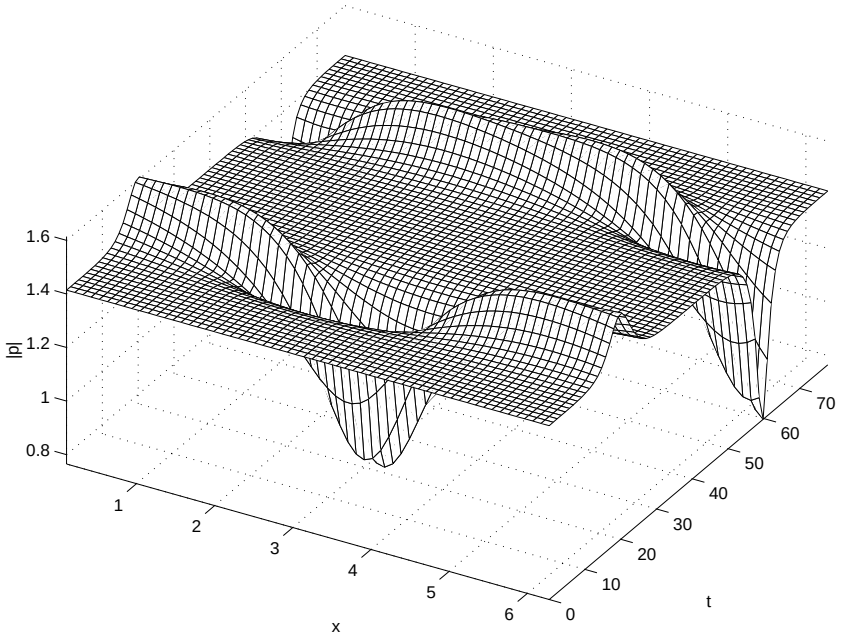

Fig. 31. Evolutionary dynamics in the nonlocal manifold near the plane wave instability — *outside* the homoclinic orbit (p-channel).

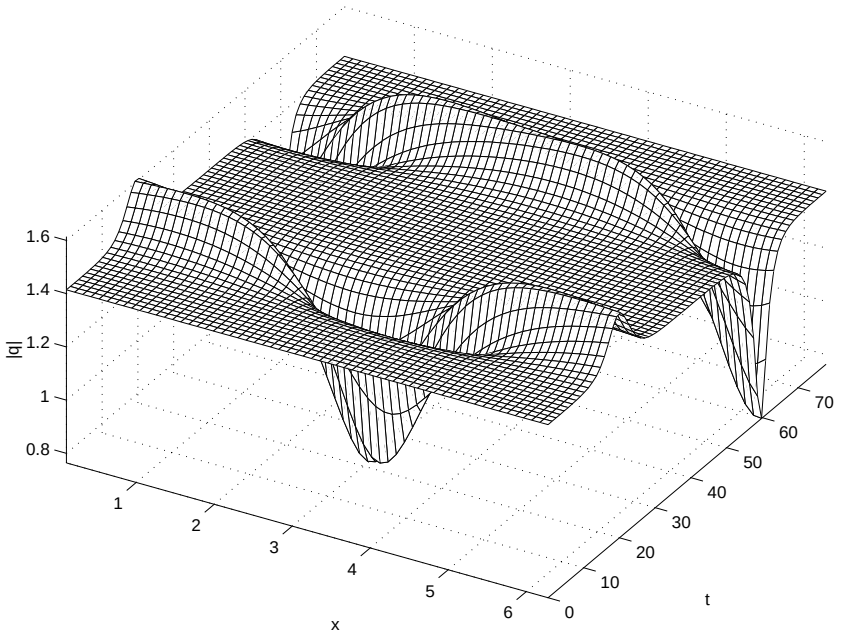

Fig. 32. Evolutionary dynamics in the nonlocal manifold near the plane wave instability — *outside* the homoclinic orbit (q-channel).

The integrals of the coupled pair of stationary equations can be eliminated and the resulting set of differential equations numerically integrated along space and time characteristics using the standard Runge-Kutta fourth order scheme. The presence of a crossed homoclinic saddle in the phase space of the CNLS system (qualitatively similar to that of the unforced Duffing oscillator), can be seen by perturbing the critical solution first by $\pm(v_1 + v_2)$, resulting in orbits corresponding to the interiors of the two homoclinic loops, as shown in Figures 25, 26, 27, and 28. Orbits on the exterior of the saddle can be produced by perturbations of the type $\pm(v_1 - v_2)$, as shown in Figures 29, 30, 31, and 32.

Conclusion

The intermediate wavelength nature of the defocusing instability agrees qualitatively with the instability observed by Rothenberg [33] experimentally and in numerical simulations of the buildup of modulational instability in nonintegrable CNLS fields.

In particular, the cross-phase nature of the new instability and its saturation in the neighbourhood of crossed homoclinic saddles in both the focusing and defocusing CNLS equations is clearly distinguished from the long-wave, self-phase instability of the focusing equation. Genuine nonlinear and nonlocal trajectories homoclinic to unstable plane waves are constructed and visualized using Bäcklund transformations and the stationary equations of the integrable CNLS equations. In addition, an important correspondence between unstable linear eigenmodes and the Floquet spectral data of the integrable Lax pair for the CNLS system is established, similar to results of Forest and Lee [18] for the scalar NLS equation. Several developments of the scalar NLS theory remain open for the CNLS system.

References

[1] Ablowitz, M. J., Kaup, D. J., Newell, A. C., and Segur, H., *The inverse scattering transform — Fourier analysis of nonlinear problems*, Stud. Appl. Math., **53**:249–315 (1974).
[2] Adams, M. R., Harnad, J., Previato, E., *Isospectral Hamiltonian flows in finite and infinite dimensions*, Commun. Math. Phys., **117**:451–500 (1988).
[3] Adams, M. R., Harnad, J., Hurtubise, J., *Darboux coordinates and Liouville-Arnold integration in loop algebras*, Commun. Math. Phys., **155**:385–413 (1993).
[4] Adams, M. R., Harnad, J., Hurtubise, J., *Isospectral Hamiltonian flows in finite and infinite dimensions II*, Commun. Math. Phys., **134**:555–585 (1990).
[5] Agrawal, G. P., *Modulation instability induced by cross-phase modulation*, Phys. Rev. Lett., **59**:880–883 (1987).
[6] Agrawal, G. P., *Nonlinear Fiber Optics*, Academic Press, San Diego (1989).
[7] Beals, R., Deift, P., Tomei, C., *Inverse scattering for self-adjoint-nth order differential-operators on the line*, Lect. Notes Math., 1285:26–38 (1987).
[8] Beals, R., Sattinger, D. H., *On the complete-integrability of completely integrable systems*, Commun. Math. Phys., **138**:(3) 409–436 (1991).
[9] Benjamin, T. B., and Feir, J. E., *The disintegration of wave trains in deep water*, J. Fluid Mech., **27**:417–430 (1967).
[10] Benney, D. J., and Newell, A. C., *The propagation of nonlinear wave envelopes*, J. Math. Phys., **46**:133 (1967).

[11] Blow, K. J., Doran, N. J., and Wood, D., *Polarization instabilities for solitons in birefringent fibers*, Opt. Lett., **12**:202 (1987).
[12] Chen, H., *Relation between Bäcklund transformations and inverse scattering problems*, Lect. Notes Math., No. 515, 241–252.
[13] Ercolani, N., Forest, M. G., *The geometry of real Sine-Gordon wavetrains*, Commun. in Math. Phys., **99**, 1–49 (1985).
[14] Ercolani, N., Forest, M. G., McLaughlin, D. W., *The origin and saturation of modulational instabilities*, Physica D, **18**:472–474 (1986).
[15] Ercolani, N., Forest, M. G., McLaughlin, D. W., *Geometry of the modulational instability. 3. Homoclinic orbits for the Periodic Sine-Gordon equation*, Physica D, **43**:(2–3) 349–384, 1990.
[16] Ercolani, E. M., and McLaughlin, D. W., *Toward a topological classification of integrable PDE's*, in *The Geometry of Hamiltonian Systems*, ed. T. Ratiu, MSRI 22, 111–128, Springer-Verlag, New York, 1991.
[17] Forest, M. G., and McLaughlin, D. W., *Spectral theory for the periodic Sine-Gordon equation: A concrete viewpoint*, J. Math. Phys., **23**:1248–1277 (1982).
[18] Forest, M. G., and Lee, J. E., *Geometry and modulation theory for the periodic Schrödinger equation*, in *Oscillation Theory, Computation, and Methods of Compensated Compactness*, eds. Dafermos, et al., *I.M.A. in Math and Its Applications*, **2**:35–70, Springer-Verlag, New York, 1986.
[19] Hasegawa, A., *Optical Solitons in Fibers*, Springer-Verlag, New York (1989).
[20] Hasegawa, A., and Kodama, Y., Solitons in Optical Communications, Clarendon Press, Oxford, 1995.
[21] Hasegawa, A., and Tappert, F., *Transmission of stationary nonlinear optical pulses in dispersive dielectric fibers*, Appl. Phys. Lett., **23**:142 (1973).
[22] McKean, H., *Boussinesq's equation on the circle*, Commun. Pure and Appl. Math., **34**:599–691 (1981).
[23] McLaughlin, D. W., and Overman, E. A., *Whiskered tori for integrable pde's: Chaotic behaviour in near integrable pde's*, in *Surveys in Applied Mathematics*, Vol. 1, Chapter 2, eds. Keller, et al., Plenum Press, New York, 1995.
[24] McLaughlin, D. W., and Li, Y., *Morse and Melnikov functions for Nls Pdes*, Commun. Math. Physics, **162**:(1) 175–214 (1994).
[25] Manakov, S. V., ZETP **65**, 505 (1973).
[26] Menyuk, C. R., *Nonlinear pulse propagation in birefringent optical fibers*, IEEE J. Quantum Electron., **23**:174 (1987).
[27] Miura, R. M., and Kruskal, M. D., *Application of a nonlinear WKB method to the Korteweg-de Vries equation*, SIAM J. Appl. Math., **26**:376–395 (1974).
[28] Moser, J., *Geometry of quadrics and spectral theory*, The Chern Symposium 1979, Hsiang, W. Y., et al., Springer-Verlag, New York, 1980.
[29] Newell, A. C., *Solitons in Mathematics and Physics*, S.I.A.M., Philadelphia, 1985.
[30] Previato, E., *Monodromy of Boussinesq elliptic operators*, Acta Applicandae Mathematicae, **36**:49–55 (1994).
[31] Roske, G. J., *Some nonlinear multiphase reactions*, Stud. Appl. Math., **55** 231–238 (1976).
[32] Rothenberg, J. E., *Modulational instability for normal dispersion*, Phys. Rev. A, **42**:682–685 (1990).
[33] Rothenberg, J. E., *Observation of the buildup of modulational instability from wavebreaking*, Opt. Lett., **16**:18–20 (1991).
[34] Sattinger, D. H., and Zurkowski, V. D., *Gauge-Theory of Bäcklund Transformations.2*, Physica D, **26**:(1–3) 225–250 (1987).
[35] Sheu, S-P., Bäcklund transformations and homoclinic solutions for the nonlinear Schrodinger system, Ph.D. thesis, Ohio State University, 1992.
[36] Tracy, E. R., Chen, H. H., *Nonlinear self-modulation: An exactly solvable model*, Phys. Rev. A, **37**(3):815–839 (1988).
[37] Tracy, E. R., Chen, H. H., Lee, Y. C., *Study of quasiperiodic solutions of the nonlinear Schrödinger equation and the nonlinear modulational instability*, Phys. Rev. Lett., **53**(3)218–221 (1984).

[38] Wai, A., *Nonlinear Processes in Physics: Proceedings of III Potsdam-V Kiev Workshop*, Springer-Verlag, Berlin, 1991.
[39] Whitham, G. B., *Nonlinear dispersive waves*, Proc. Roy. Soc. A, **283**:238–261 (1965).
[40] Wright, O. C., *Modulational instability in a defocussing coupled nonlinear Schrödinger system*, Physica D, **82**:1–10 (1995).
[41] Wright, O. C., *The stationary equations of a coupled nonlinear Schrödinger system*, to appear, Physica D.
[42] Yang, J., and Benney, D. J., *Some properties of nonlinear wave systems*, Stud. Appl. Math., **96**:111–139 (1996).
[43] Yang, J., *Coherent structures in weakly birefringent optical fibers*, Stud. Appl. Math., **97**:127–148 (1996).